# Plant-derived stilbenoids as DNA-binding agents: from monomers to dimers

Chiara Platella,[a],+ Stefania Mazzini,[b],+ Ettore Napolitano,[a] Luce M. Mattio,[b] Giovanni Luca Beretta,[c] Nadia Zaffaroni,[c] Andrea Pinto,[b] Daniela Montesarchio,[a],* Sabrina Dallavalle[b]

[a]*Department of Chemical Sciences, University of Naples Federico II, via Cintia 21, 80126 Naples, Italy*

[b]*Department of Food, Environmental and Nutritional Sciences (DeFENS), Università degli Studi di Milano, via Celoria 2, 20133 Milan, Italy*

[c]*Molecular Pharmacology Unit, Department of Applied Research and Technological Development, Fondazione IRCCS Istituto Nazionale Tumori, via Amadeo 42, 20133 Milan, Italy*

[+]These authors contributed equally to this work.

*To whom correspondence should be addressed. Tel: +39 081 674126; Fax: +39 081 674313; Email: daniela.montesarchio@unina.it

## Abstract

Stilbenoids are natural compounds endowed with several biological activities, including cardioprotection and cancer prevention. Among them, (±)-*trans*-δ-viniferin, deriving from *trans*-resveratrol dimerization, was here investigated in its ability to target DNA duplex and G-quadruplex structures by exploiting NMR, circular dichroism, fluorescence spectroscopy and molecular docking. (±)-*trans*-δ-Viniferin proved to bind both the minor and major grooves of duplexes, whereas it bound the 3'- and 5'-ends of a G-quadruplex by stacking on the outer quartets, accompanied by rearrangement of flanking residues. Noteworthy, (±)-*trans*-δ-viniferin demonstrated higher affinity for the investigated DNA targets than its monomeric counterpart. Additionally, the methoxylated derivatives of (±)-*trans*-δ-viniferin and *trans*-resveratrol, i.e. (±)-pterostilbene-*trans*-dihydrodimer and *trans*-pterostilbene respectively, were evaluated, revealing similar binding modes, affinities and stoichiometries with the DNA targets as their parent analogues. All the tested compounds were cytotoxic at μM concentration on several cancer cell lines and showed DNA damaging activity, consistent with their ability to tightly interact with duplex and G-quadruplex structures.

## Introduction

Phenolic compounds are a class of plant secondary metabolites widely present in fruits, vegetables and legumes.[1,2] Over 8000 natural phenolic products have been described in edible plants,

representing an important part of our diet as they are the most abundant antioxidants consumed by humans.[3]

Among natural phenolic compounds, stilbenoids are largely found in several fruits and crops, including blueberries, cranberries, peanuts and grapes.[4] Stilbenoids are both woody constitutive metabolites and phytoalexins, substances produced by plants in response to biotic and abiotic stress factors, such as microbes and fungi infections, UV radiations, physical trauma.[5] They share a common structure generally constituted by a C6–C2–C6 unit, i.e. a 1,2-diphenylethylene moiety, with aromatic rings carrying one or more hydroxy groups. In the last decades, stilbenoids have been largely studied because of their diverse bioactivities, comprising cardioprotection, neuroprotection, anti-diabetic and anti-inflammatory properties, cancer prevention and treatment,[6] with *trans*-resveratrol and its methoxylated analogue *trans*-pterostilbene (Figure 1A,B) being the most deeply investigated stilbenoids.[7–11]

A number of recent studies, covering a myriad of models, from cell cultures to animal studies, as well as human clinical trials, have brought to the fore their potential as anticancer compounds, mainly acting through epigenetic mechanisms.[12–18] Epigenetics regulates the genetic code at several levels. Among these are DNA changes, which include modifications to DNA methylation state, histones methylation, acetylation, ubiquitination and phosphorylation, and non-coding RNA changes.

In this context, implications of G-quadruplex formation in genomic DNA for epigenetic (re)programming and chromatin remodeling have been recently considered.[19] G-quadruplexes are nucleic acid secondary structures originating from guanine-rich oligonucleotide sequences which produce stacked arrangements of G-quartets stabilized by Hoogsteen hydrogen bonding. Compared to duplex DNA, G-quadruplexes exhibit higher structural polymorphism and can adopt various topologies, i.e. parallel, antiparallel and hybrid. These structures have received significant attention as potential therapeutic targets.[20,21] Indeed, G-quadruplexes are found in the promoter regions of several genes associated with the development of cancer (e.g. c-myc, bcl-2 and c-kit oncogenes), where stabilization of the folded G-quadruplexes due to ligand interactions is proposed to inhibit the binding of transcription factors, leading to downstream silencing of oncogene expression.[22–24] Notably, also human telomeric sequences are able to form G-quadruplex structures that are not recognized by telomerase, enzyme involved in telomere elongation. Since telomerase expression is upregulated in cancer cells, the discovery of ligands able to stabilize telomeric G-quadruplex structures represent an appealing strategy for targeted anticancer therapies.[25]

Several groups have reported that *trans*-resveratrol and its analogues, in addition to producing DNA damage, activate DNA repair mechanisms in various cancer cell lines, including prostate, colon and breast cancer cells.[26–28]

In this context, some of us have recently investigated the binding of *trans*-resveratrol and its natural precursor *trans*-polydatin to various DNA model systems forming duplex or G-quadruplex structures. The biological effects of *trans*-resveratrol and *trans*-polydatin on melanoma cells well correlated with the biophysical data, proving that the interactions with DNA, observed for both compounds, can be somehow involved in the mechanisms explaining their anticancer activity.[29,30] In particular, *trans*-resveratrol was found to induce higher antiproliferative effects, higher inhibition of telomerase activity and more efficient reduction of the expression of c-myc oncogene compared to *trans*-polydatin.

Encouraged by these results on the monomeric stilbenoid *trans*-resveratrol, the DNA interactions and related activity on cancer and normal cells have been here in-depth investigated for the dimeric derivative thereof, i.e. (±)-*trans*-δ-viniferin (Figure 1C). This product, obtained through *trans*-resveratrol self-condensation, has a three-dimensional skeleton which is intrinsically endowed with a higher number of functional groups and higher structural complexity than *trans*-resveratrol itself, thus showing in principle higher potential for selective binding to a specific target. Additionally, the methoxylated analogues of both *trans*-resveratrol and (±)-*trans*-δ-viniferin, i.e. *trans*-pterostilbene and (±)-pterostilbene-*trans*-dihydrodimer (Figure 1D) respectively, have been also synthesized according to reported procedures[31] and here examined for comparison.

In detail, (±)-*trans*-δ-viniferin as well as the pure enantiomers (*R*,*R*)-*trans*-δ-viniferin and (*S*,*S*)-*trans*-δ-viniferin[32] have been studied in their interaction with B-DNA duplex and G-quadruplex models by NMR, circular dichroism (CD), fluorescence spectroscopy and molecular docking, and compared in their binding behaviour to *trans*-resveratrol, *trans*-pterostilbene and (±)-pterostilbene-*trans*-dihydrodimer. Then, biological assays have been performed to evaluate both the antiproliferative effects on cancer and normal cells and the DNA damage ability of the dimeric and monomeric stilbenoids. Altogether these data allowed a deep insight into the capacity of these compounds to bind different DNA models, in duplex as well as in G-quadruplex form, which will be helpful for the design of novel selective DNA targeting drugs based on stilbenoid derivatives.

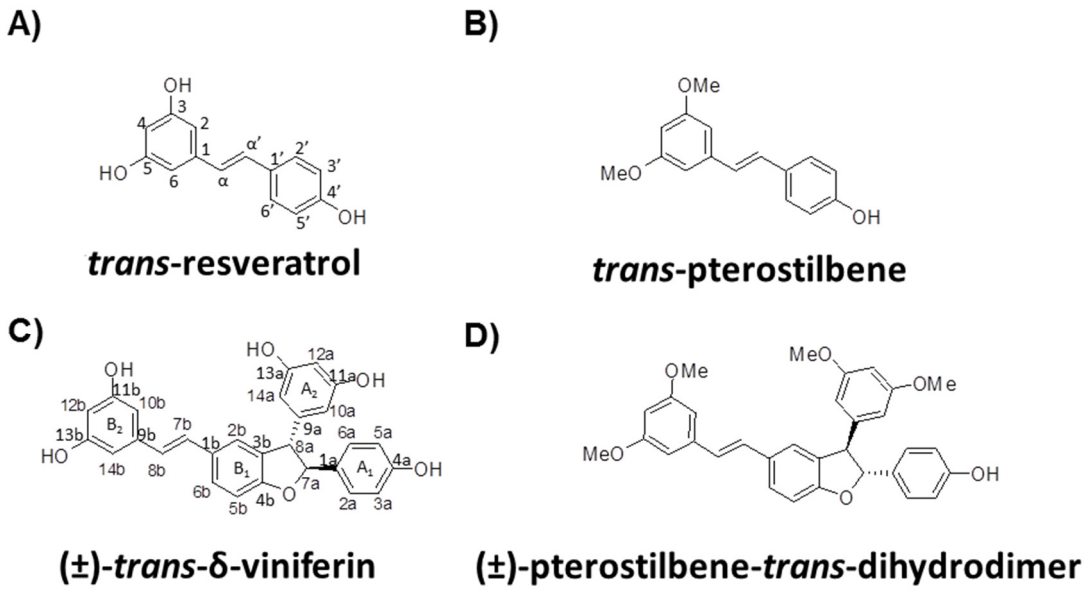


**Figure 1.** Chemical structures of A) *trans*-resveratrol, B) *trans*-pterostilbene, C) (±)-*trans*-δ-viniferin and D) (±)-pterostilbene-*trans*-dihydrodimer. Atom and ring numbering used in this study are reported in A) and C) according to Wilkens *et al.*[33]

## Results

### NMR studies

To gain structural insights into the interactions of (±)-*trans*-δ-viniferin with both DNA duplex and G-quadruplex models, $^{31}$P and $^{1}$H NMR experiments were performed.

#### *$^{31}$P and $^{1}$H NMR experiments on (±)-trans-δ-viniferin with B-DNA duplex models*

The self-complementary oligonucleotides d(CGTACG)$_2$ (forming the duplex structure here named ds6) and d(AAGAATTCTT)$_2$ (forming the duplex structure here named ds10) were used as models for CG- and AT-rich sequences, respectively. Folding of these oligomers into a duplex conformation was obtained at 15 °C in 110 mM $Na^+$-containing buffer. The $^{1}$H NMR spectra displayed signals in a region ranging from 12.4 to 13.9 ppm that were attributed to the imino protons involved in the CG and AT Watson-Crick base pairs. In particular, only two and three signals were detected for ds6 and ds10 duplexes, respectively, because of the fraying process of the terminal base pairs (Figure S1A,B, bottom).

It is known that monitoring $^{31}$P resonance is a sensitive method to detect changes in the *alfa* = O(3')-P–O(5')-C(5') and *zeta* = C(3')-O(3')–P-O(5') angles of the oligonucleotides from a *gauche-gauche* conformation (-60°, -90°) to a *gauche-trans* conformation (-60°, +180°) when an intercalation process occurs. Even small conformational changes at these angles are usually associated with a downfield shift up to 1.0–2.5 ppm for $^{31}$P resonances.[34,35] The $^{31}$P spectra acquired upon addition of (±)-*trans*-

δ-viniferin to a solution of ds6 duplex, at different ratios R = [(±)-*trans*-δ-viniferin]/[DNA], did not show shift variation of any signal (Figure 2A and Table 1). Moreover, in the titration experiment, the $^{1}$H NMR spectra showed only generalized line broadening without displaying chemical shift changes (Figures S1A and S2 and Table S1). This behavior suggested that complex equilibria, intermediate-to-fast on the NMR time scale, occurred among multiple, different species in solution. Consistently with the generalized line broadening observed in 1D-NMR spectra, no intermolecular Nuclear Overhauser Effect (NOE) contacts between (±)-*trans*-δ-viniferin and ds6 duplex were observed in 2D-NOESY experiments.

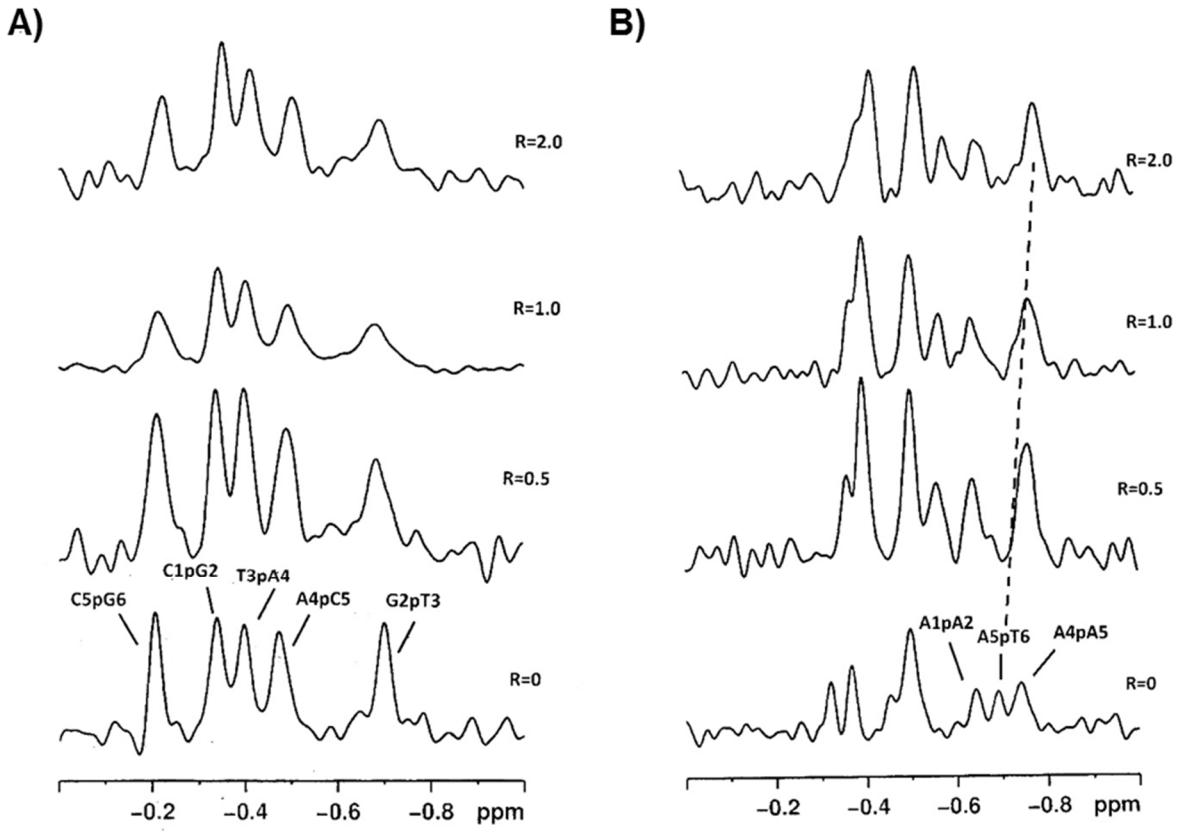


**Figure 2.** $^{1}$H-decoupled $^{31}$P NMR spectra of A) ds6 and B) ds10 duplexes treated with (±)-*trans*-δ-viniferin at 15 °C in $H_2O/D_2O$ (9:1), 100 mM NaCl, 10 mM sodium phosphate buffer (pH 7.0), at different ratios R = [(±)-*trans*-δ-viniferin]/[DNA]. Dashed line in B) indicates the upfield shift of the A5pT6 signal.

**Table 1.** $^{31}$P NMR chemical shift assignments of the signals in the free ds6 or ds10 duplex and in their complexes with (±)-*trans*-δ-viniferin[a,b].

| ds6 | | Δδ[c] | ds10 | | Δδ[c] |
|---|---|---|---|---|---|
| C1pG2 | -0.35 | 0.00 | A1pA2 | -0.65 | +0.04 |
| G2pT3 | -0.70 | 0.00 | A2pG3 | -0.38 | -0.07 |
| T3pA4 | -0.40 | 0.00 | G3pA4 | -0.50 | 0.00 |
| A4pC5 | -0.50 | -0.01 | A4pA5 | -0.80 | -0.05 |
| C5pG6 | -0.22 | -0.02 | A5pT6 | -0.80 | -0.10 |
| | | | T6pT7 | -0.57 | -0.07 |
| | | | T7pC8 | -0.40 | +0.03 |
| | | | C8pT9 | -0.50 | 0.00 |
| | | | T9pT10 | -0.40 | -0.05 |

[a]Measured at 15 °C in $H_2O/D_2O$ (9:1), 100 mM NaCl, 10 mM sodium phosphate buffer (pH 7.0) and R = 2.0.
[b]Measured in ppm from external DSS.
[c]$\Delta\delta = \delta_{bound} - \delta_{free}$.

$^1$H and $^{31}$P NMR titration experiments performed with ds10 duplex gave different results: although also in this case no relevant chemical shift variation was detected in $^1$H NMR spectra (Figures S1B and S3), the signals belonging to its $^{5'}$AATT$^{3'}$ tract were slightly perturbed (Table S1). The $^{31}$P NMR spectra did not show downfield chemical shift variations of the signals indicating that no major, significant change in the backbone of the oligonucleotide occurred. Nevertheless, the signal attributed to A5pT6 experimented a small upfield chemical shift variation (Figure 2B and Table 1).

To get a deeper insight into the interactions between (±)-*trans*-δ-viniferin and ds10 duplex, 2D-NOESY experiments were performed. The resonances of (±)-*trans*-δ-viniferin in the complex were attributed by TOCSY and ROESY experiments on the basis of the resonances of the free ligand (Figure S4 and Table S2). (±)-*trans*-δ-Viniferin signals were mostly overlapped to anomeric protons of the oligomer. However, ligand protons at δ 6.79 (H3,5a), 6.42 (H10,14b) and 5.42 (H7a) ppm showed NOEs contacts with H2 and H1' protons of A and T units in the $^{5'}$AATT$^{3'}$ tract, located in the minor groove of the duplex (Figure 3 and Table 2). In addition, protons H3,5a and H10,14b of (±)-*trans*-δ-viniferin displayed NOE interactions with the aromatic H6 of T6 located in the major groove (Figure 3 and Table 2). No NOE cross-peaks were observed between the imino protons of ds10 duplex and the ligand protons.

Overall, these findings allowed excluding an intercalative binding mode in the interaction of (±)-*trans*-δ-viniferin with the two investigated duplex models. On the other hand, binding to both minor and major grooves appeared to be the preferential binding mode of (±)-*trans*-δ-viniferin to ds10 duplex, while the line broadening of $^1$H NMR signals together with the absence of NOE interactions did not allow to get detailed information about the preferred binding sites of (±)-*trans*-δ-viniferin on the ds6 duplex.

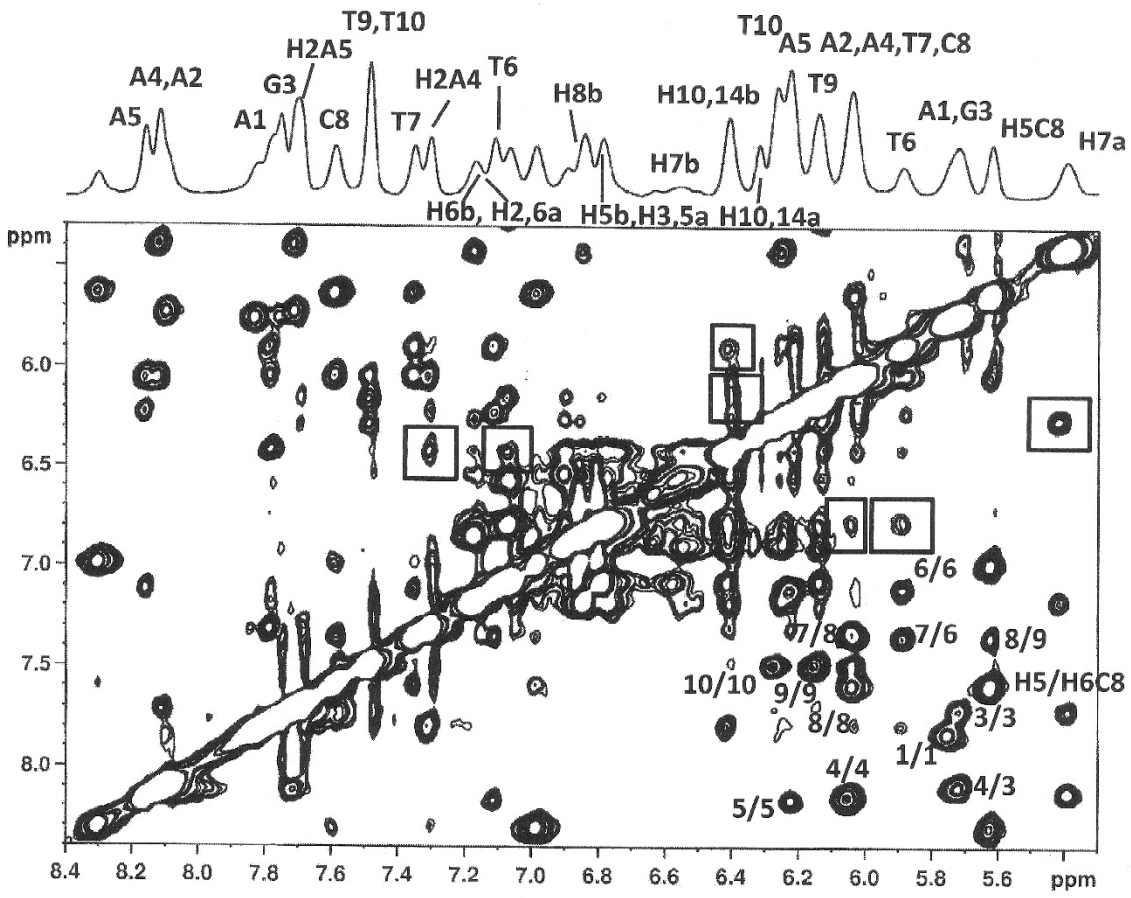


**Figure 3.** Selected region of 2D-NOESY spectrum of ds10 duplex treated with (±)-*trans*-δ-viniferin at 15 °C in $H_2O/D_2O$ (9:1), 100 mM NaCl, 10 mM sodium phosphate buffer (pH 7.0), at R = [(±)-*trans*-δ-viniferin]/[DNA]=2.0. The numbers indicate intra- and inter-residue NOE interactions. The boxes indicate the NOE contacts between the ligand and ds10 duplex (see Table 2).

**Table 2.** Intermolecular NOE interactions between (±)-*trans*-δ-viniferin and ds10 duplex[a,b].

| (±)-*trans*-δ-viniferin protons (ppm) | ds10 protons |
|---|---|
| H3,5a (6.79) | H1'T6 |
| H3,5a (6.79) | H1'T7 |
| H3,5a (6.79) | H6T6 |
| H7a (5.42) | H1'A5 |
| H10,14b (6.42) | H1'T6 |
| H10,14b (6.42) | H6T6 |
| H10,14b (6.42) | H1'T7 |
| H10,14b (6.42) | H1'A4 |
| H10,14b (6.42) | H2A4 |

[a]Measured at 15 °C in $H_2O/D_2O$ (9:1), 100 mM NaCl, 10 mM sodium phosphate buffer (pH 7.0) and R = 2.0.
[b]Measured in ppm from external DSS.

*$^{1}$H NMR experiments of* (±)-*trans*-δ-viniferin *with a G-quadruplex model*

The imino proton signals of G-quadruplex-forming oligonucleotides are correlated with their well-defined global structure. The parallel G-quadruplex Pu22T14T23, originating from c-myc oncogene promoter of sequence d(TGAGGGTGGGTAGGGTGGGTAA), comprising two G to T mutations, was chosen as a target model because it gave higher quality spectra in $K^+$ solution in comparison to the wild-type oligonucleotide (Figure 4A). Notably, Pu22T14T23 has already proved to be a good model to study G-quadruplex/ligand interactions.[23,36] Twelve imino proton signals were observed and assigned (Figure 4B, bottom),[23] consistent with the formation of a G-quadruplex structure composed of three stacked quartets.[36]

$^{1}$H NMR titration experiments were performed by adding increasing amounts of (±)-*trans*-δ-viniferin to the G-quadruplex solution with ratios R = [(±)-*trans*-δ-viniferin]/[DNA] ranging from 0 to 2.0. A single new set of only nine imino proton signals, because of some overlapping, was observed at R = 2.0 (Figure 4B). This suggested that well-defined DNA/ligand complexes were present in our conditions and allowed assigning imino and aromatic protons by 2D-NOESY spectra (Table S3). In the NOESY spectrum, the sequential and imino proton inter-residue NOE interactions of Pu22T14T23 G-quadruplex in the complex with (±)-*trans*-δ-viniferin were detected (Table S4 and Figures S5 and S6). The addition of (±)-*trans*-δ-viniferin caused perturbations to the chemical shifts of the imino protons (Figure 4B and Table S3), giving a first indication that an interaction between (±)-*trans*-δ-viniferin and Pu22T14T23 G-quadruplex occurred. In particular, signals belonging to both 3'-end (G9, G18 and G22) and 5'-end (G16) quartets, as well as to G17 in the middle quartet, were the most shifted ones. In detail, the imino protons of G16, G17 and G18 in the complex with (±)-*trans*-δ-viniferin experimented upfield variations, whereas for G9 and G22 downfield variations were observed. Considering that typical end-stackers have been reported to induce upfield shifts in the guanine residues of quartets in the G-quadruplex NMR spectra,[23,36] the chemical shift changes induced by (±)-*trans*-δ-viniferin reflect the complexity of the ligand interaction with the G-quadruplex (see fluorescence spectroscopy experiments and molecular modeling sections).

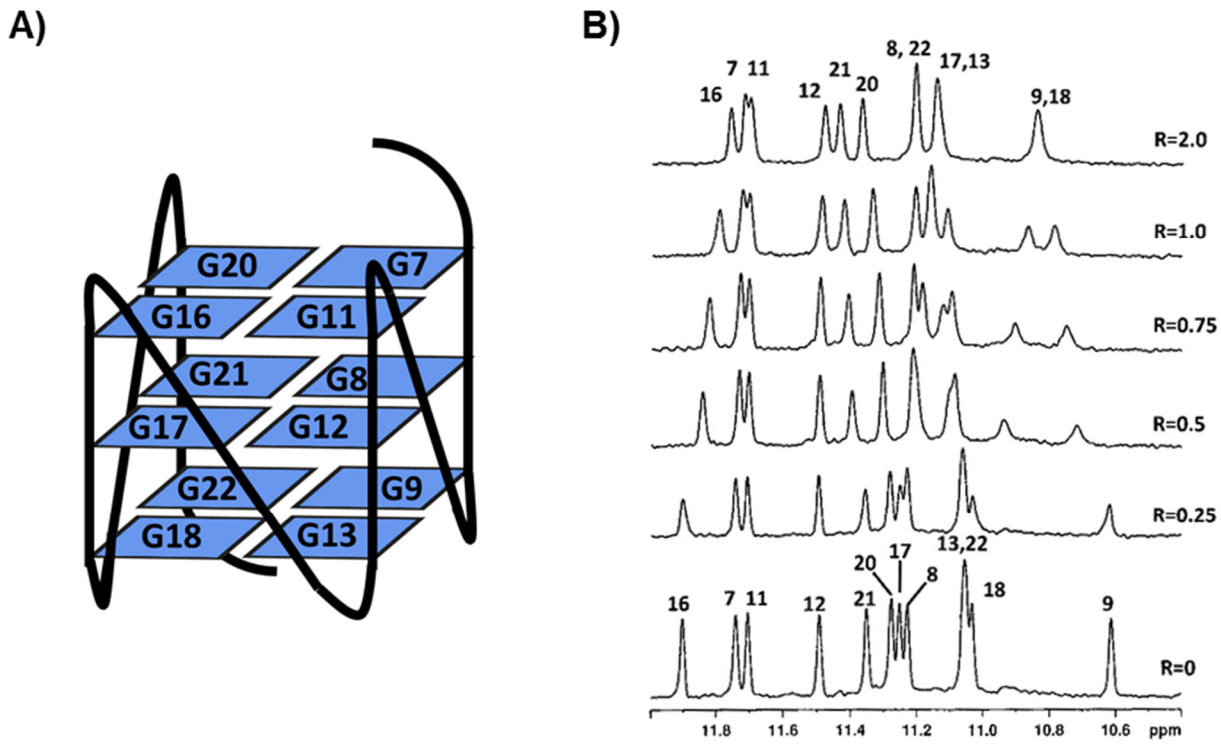


**Figure 4.** A) Schematic representation of Pu22T14T23 G-quadruplex. B) Imino proton region of the $^{1}$H NMR titration spectra of Pu22T14T23 G-quadruplex with (±)-*trans*-δ-viniferin at 25 °C in $H_2O/D_2O$ (9:1), 70 mM KCl, 25 mM potassium phosphate buffer (pH 6.9), at different ratios R = [(±)-*trans*-δ-viniferin]/[DNA].

The 5'- and 3'-end flanking residues did not present NOE contacts with the ligand, whereas some chemical shift variations were observed for 3'-end flanking residues, suggesting a rearrangement of this segment induced by the ligand. In detail, while protons of A6 at 5'-end did not experiment chemical shift variations, thus indicating that A6 was still stacked on G7,[37] T23 methyl protons underwent a downfield shift variation, proving a partial de-stacking of T23 upon addition of the ligand. Additionally, the downfield shift observed for A24 and G9 protons suggested that A24 was no more involved in stacking with the T23:A25 base pair, and A25 was no more folded over the G9 aromatic moiety, as observed in the free Pu22 G-quadruplex structure.[37] Conversely, no relevant chemical shift changes were detected for the residues located in the loops of the G-quadruplex, i.e. T10, T14, A15 and T19 (Table S3). Moreover, new broad peaks were detected upon ligand addition in the range of 5.5-6.8 ppm that were attributed to the protons of (±)-*trans*-δ-viniferin. Their broad shape indicated that the ligand could move in the binding site (Figure 5). Unfortunately, the overlapping between the signals of G-quadruplex deoxyribose moieties protons and (±)-*trans*-δ-viniferin protons prevented the unambiguous assignment of the protons belonging to the ligand. Nevertheless, few intermolecular NOE contacts with imino protons of G9, G13, G16 and G18 were

detected (Figure S7). These NOEs were in agreement with the relatively large chemical shift perturbation observed in $^1$H NMR spectra for these residues.

Overall, these findings suggested that the binding of (±)-*trans*-δ-viniferin did not disrupt the original parallel fold of the Pu22 G-quadruplex. However, rearrangements of the flanking residues covering the external quartets were observed as a consequence of the ligand binding at both the 3'- and 5'-end quartets through stacking mode.

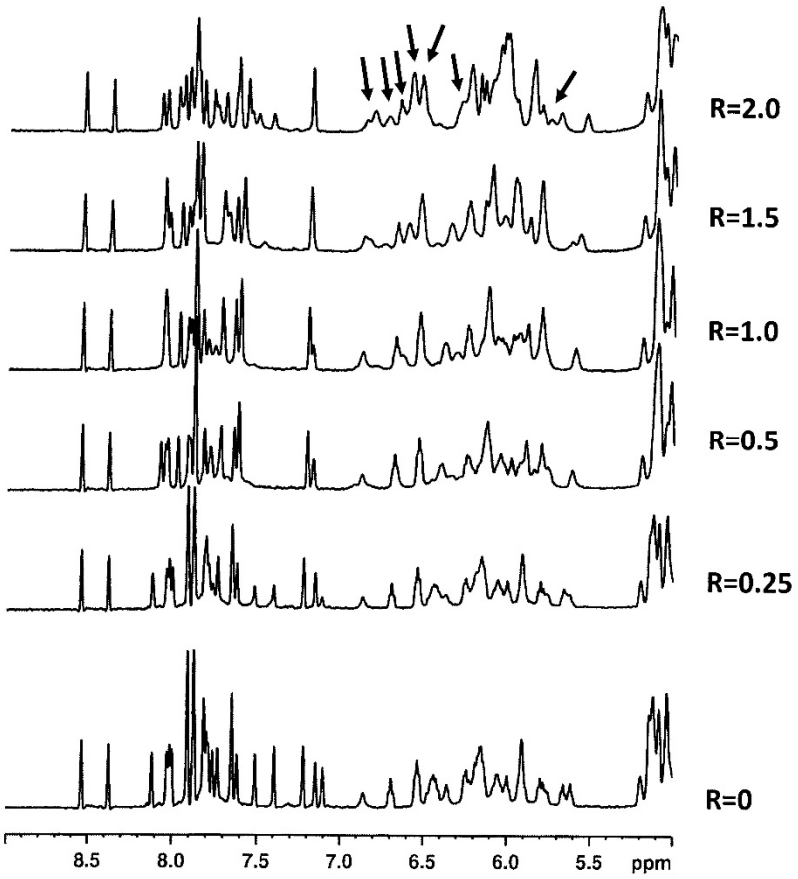


**Figure 5.** Aromatic and anomeric protons region of the $^1$H NMR titration spectra of Pu22T14T23 G-quadruplex with (±)-*trans*-δ-viniferin at 25 °C in $H_2O/D_2O$ (9:1), 70 mM KCl, 25 mM potassium phosphate buffer (pH 6.9), at different ratios R = [(±)-*trans*-δ-viniferin]/[DNA]. The arrows indicate the (±)-*trans*-δ-viniferin signals.

**Circular dichroism experiments**

Circular dichroism experiments were performed on ds6 and ds10 duplexes and Pu22T14T23 G-quadruplex in the absence and presence of (±)-*trans*-δ-viniferin, *trans*-resveratrol, *trans*-pterostilbene and (±)-pterostilbene-*trans*-dihydrodimer to assess the effects of these ligands on different DNA secondary structures. The pure enantiomers (*R*,*R*)-*trans*-δ-viniferin and (*S*,*S*)-*trans*-δ-viniferin were also studied in order to investigate the role of chirality in the DNA binding ability of this ligand. First, CD spectra and CD-melting experiments were carried out on ds6 and ds10 duplexes and Pu22T14T23 G-quadruplex alone to characterize the CD behaviour of the three DNA models of choice. The analysis of CD spectra indicated that ds6 and ds10 folded into duplexes adopting B-conformation, featured by a maximum at 279 or 278 nm and a minimum at 257 or 248 nm respectively (Figure S8A,B), while Pu22T14T23 folded into a parallel G-quadruplex, featured by a maximum at 265 nm and a minimum at 244 nm (Figure S8C, black line), confirming the expected conformations for these duplex and G-quadruplex structures under the here used conditions,[38,39] i.e. 110 mM $Na^+$- or 95 mM $K^+$-containing buffer for duplexes or G-quadruplex, respectively. The CD-melting experiments, recorded by following the CD changes at the wavelength of intensity minimum or maximum characteristic of each DNA secondary structure, allowed determining $T_m$ values of 18, 22 and ca. 92 (±1) °C for ds6, ds10 duplexes and Pu22T14T23 G-quadruplex, respectively (Figure S9A-C, black lines). Due to the low accuracy of the melting temperature of Pu22T14T23 G-quadruplex determined in the above conditions, Pu22T14T23 G-quadruplex was studied alone and in its interaction with the different ligands in a buffer containing a lower concentration of potassium ions, i.e. 10 mM. Under these conditions, Pu22T14T23 still folded in a parallel G-quadruplex structure showing the same CD signature as observed at higher $K^+$ concentration (Figure S8C, red line), but with the remarkably lower $T_m$ of 75 (±1) °C (Figure S9C, red line). Then, solutions of ds6 and ds10 duplexes or Pu22T14T23 G-quadruplex were titrated with increasing amounts of each ligand and CD spectra recorded after each addition (Figures S10-S15). The contribution of the chiral ligands (*R,R*)-*trans*-δ-viniferin and (*S,S*)-*trans*-δ-viniferin, even if of low intensity (data not shown), was taken into consideration and subtracted at each titration point for all the systems containing the two pure enantiomers (Figures S11 and S12). No significant variation of the CD profiles was observed for any of the investigated systems (Figures S10-S15), thus proving that the overall folds of the here studied duplexes and G-quadruplex were preserved even upon ligand binding, consistently with the NMR results.

CD-melting experiments were also performed to evaluate the effects on the ds6 and ds10 duplexes or Pu22T14T23 G-quadruplex thermal stability upon incubation with each of the investigated ligands. CD-melting curves were recorded in the presence of each ligand at 1:4 DNA:ligand ratio (Figures

S16 and S17). The $T_m$ and $\Delta T_m$ values for each of the investigated systems are reported in Table 3. No significant stabilizing effects were observed on ds6 duplex, with the only exception of (*R,R*)-*trans*-δ-viniferin ($\Delta T_m$ = +2 °C). On the other hand, slight stabilizing effects were induced by (±)-δ-*trans*-viniferin, (*R,R*)-*trans*-δ-viniferin, (*S,S*)-*trans*-δ-viniferin and *trans*-resveratrol on Pu22T14T23 G-quadruplex ($\Delta T_m$ = +1 °C), while *trans*-pterostilbene or (±)-pterostilbene-*trans*-dihydrodimer induced no stabilization of Pu22T14T23 G-quadruplex. Notably, the highest stabilizing effects were detected for all the ligands on ds10 duplex. Interestingly, (±)-*trans*-δ-viniferin was able to stabilize ds10 duplex slightly more ($\Delta T_m$ = +4 °C) than the single pure enantiomers (*R,R*)-*trans*-δ-viniferin ($\Delta T_m$ = +2 °C) and (*S,S*)-*trans*-δ-viniferin ($\Delta T_m$ = +3 °C). A similar stabilization as found for (±)-δ-*trans*-viniferin was observed for *trans*-resveratrol and *trans*-pterostilbene ($\Delta T_m$ = +4 °C), while (±)-pterostilbene-*trans*-dihydrodimer produced only a slight increase of $T_m$ of ds10 duplex ($\Delta T_m$ = +2 °C), revealing minor stabilizing effects on this DNA sequence.

**Table 3.** Melting temperatures ($T_m$) for solutions of ds6 and ds10 duplexes and Pu22T14T23 G-quadruplex in the absence and presence of 4 molar equivalents of each ligand. Each $\Delta T_m$ was calculated as the difference between $T_m$ of 1:4 DNA/ligand ratio system and $T_m$ of DNA alone.

| | **$T_m$ (°C) (±1)** | | | **$\Delta T_m$ (°C)** | | |
|---|---|---|---|---|---|---|
| **Ligand/DNA target** | **ds6** | **ds10** | **Pu22T14T23** | **ds6** | **ds10** | **Pu22T14T23** |
| **No ligand** | 18 | 22 | 75 | - | - | - |
| **(±)-*trans*-δ-viniferin** | 18 | 26 | 76 | 0 | +4 | +1 |
| **(*R,R*)-*trans*-δ-viniferin** | 20 | 24 | 76 | +2 | +2 | +1 |
| **(*S,S*)-*trans*-δ-viniferin** | 18 | 25 | 76 | 0 | +3 | +1 |
| ***trans*-resveratrol** | 18 | 26 | 76 | 0 | +4 | +1 |
| ***trans*-pterostilbene** | 18 | 26 | 75 | 0 | +4 | 0 |
| **(±)-pterostilbene-*trans*-dihydrodimer** | 18 | 24 | 75 | 0 | +2 | 0 |

**Fluorescence spectroscopy experiments**

To get information about the binding stoichiometry and constants for the complexes formed between *trans*-δ-viniferin**,** *trans*-resveratrol, *trans*-pterostilbene and (±)-pterostilbene-*trans*-dihydrodimer and ds6, ds10 duplexes or Pu22T14T23 G-quadruplex, titration fluorescence experiments were

performed. In detail, stilbenoid solutions were titrated with increasing amounts of ds6 and ds10 duplexes or Pu22T14T23 G-quadruplex solutions, and, after each addition, the corresponding fluorescence spectra were recorded. A significant fluorescence enhancement was observed in all titration experiments (Figures S18-S22), except for titrations of (±)-pterostilbene-*trans*-dihydrodimer with both the investigated duplex and G-quadruplex structures, which resulted in fluorescence quenching (Figure S23). These data further corroborated the effective interaction between the here studied ligands and the duplex/G-quadruplex structures of choice. The fraction of bound ligand was then calculated from the obtained fluorescence intensity values and reported as a function of the DNA concentration. These experimental data were fitted with an independent and equivalent-sites model,[40] thus providing binding stoichiometries and constants for all DNA/ligand systems (Figures 6 and S24-S26 and Table 4). A binding stoichiometry of 1:3 DNA/ligand was found for the complexes between (±)-*trans*-δ-viniferin, (*R,R*)-*trans*-δ-viniferin, (*S,S*)-*trans*-δ-viniferin and ds6 and ds10 duplexes, as well as for the complexes between (±)-*trans*-δ-viniferin and Pu22T14T23 G-quadruplex, whereas a binding stoichiometry of 1:2 DNA/ligand was observed for (*R,R*)-*trans*-δ-viniferin and (*S,S*)-*trans*-δ-viniferin in their interaction with Pu22T14T23 G-quadruplex. Apparent binding constants of $(6.1\pm6.0) \times 10^6$, $(1.1\pm1.9) \times 10^7$ or $(1.3\pm0.9) \times 10^7$ $M^{-1}$ were found for the complexes between (±)-*trans*-δ-viniferin and ds6 and ds10 duplexes or Pu22T14T23 G-quadruplex, respectively. On the other hand, apparent binding constants of $(5.7\pm5.3) \times 10^6$, $(4.4\pm6.3) \times 10^6$ or $(1.7\pm1.5) \times 10^6$ $M^{-1}$ were obtained for the complexes between (*R,R*)-*trans*-δ-viniferin and ds6 and ds10 duplexes or Pu22T14T23 G-quadruplex, respectively, while apparent binding constants of $(1.0\pm1.4) \times 10^7$, $(1.7\pm1.0) \times 10^6$ or $(0.5\pm0.7) \times 10^6$ $M^{-1}$ were obtained for the complexes between (*S,S*)-*trans*-δ-viniferin and ds6 and ds10 duplexes or Pu22T14T23 G-quadruplex, respectively.

A binding stoichiometry of 1:1 and binding constants of $(1.6\pm1.4) \times 10^6$, $(1.6\pm1.3) \times 10^6$ or $(1.2\pm0.6) \times 10^6$ $M^{-1}$ were found for the complexes between *trans*-resveratrol and ds6 and ds10 duplexes or Pu22T14T23 G-quadruplex, respectively. The same binding stoichiometry as *trans*-resveratrol and binding constants of $(1.2\pm0.5) \times 10^6$, $(1.6\pm0.9) \times 10^6$ or $(3.9\pm0.9) \times 10^6$ $M^{-1}$ were obtained for the complexes between *trans*-pterostilbene and ds6 and ds10 duplexes or Pu22T14T23 G-quadruplex, respectively.

On the other hand, a binding stoichiometry of 1:2 was found for the complexes between (±)-pterostilbene-*trans*-dihydrodimer and all the investigated DNA oligonucleotides. Apparent binding constants of $(1.8\pm1.8) \times 10^6$, $(0.9\pm1.3) \times 10^6$ and $(1.9\pm1.5) \times 10^6$ were found for the complexes between (±)-pterostilbene-*trans*-dihydrodimer and ds6 and ds10 duplexes or Pu22T14T23 G-quadruplex, respectively.

In excellent agreement with NMR data for the G-quadruplex model here investigated, the binding stoichiometries observed for the (±)-*trans*-δ-viniferin/(*R,R*)-*trans*-δ-viniferin/(*S,S*)-*trans*-δ-viniferin:Pu22T14T23 G-quadruplex complexes - including 1:2 up to 1:3 DNA/ligand complexes - provided an additional and independent evidence in support of a stacking binding mode at both the outer Pu22T14T23 G-quadruplex quartets. Notably, the 1:2 DNA/ligand binding stoichiometry found for the (±)-pterostilbene-*trans*-dihydrodimer:Pu22T14T23 G-quadruplex complexes suggested a similar binding mode, as expected considering its structural similarity with (±)-*trans*-δ-viniferin.

The binding stoichiometry found for the (±)-*trans*-δ-viniferin/(*R,R*)-*trans*-δ-viniferin/(*S,S*)-*trans*-δ-viniferin:ds10 duplex complexes was also plausible considering the interaction of the ligands at both the minor and major grooves of ds10 duplex inferred by the NMR analysis.

Moreover, the 1:1 binding stoichiometries observed for both *trans*-resveratrol and *trans*-pterostilbene with all the investigated DNA sequences suggested a similar binding mode for these ligands to the duplex or G-quadruplex structures as a consequence of their structural similarity.

For the here studied systems featured by 1:2 or 1:3 DNA/ligand binding stoichiometries, the obtained binding constants were considered only as apparent constants. Indeed, multiple binding events inevitably result in non-equivalent binding sites of presumably different affinity and, in these cases, the independent and equivalent-sites model should be considered only as a simple reference model, not perfectly adhering to the real and more complex systems under investigation. Therefore, in the case of multiple binding events which, appearing unresolved when following spectroscopic changes, can be represented only by a simplified model based on independent and equivalent sites, as is the case, only averaged constant values over all the occurring binding events can be extrapolated.[41,42] Hence, the here obtained data allow only a rough estimation of the real binding constants, which still represent useful indications in the overall understanding of the systems under investigation.

Altogether these data proved a tight interaction between all the explored ligands and both duplex- and G-quadruplex-forming DNA oligonucleotides, with no relevant marked preference for a specific DNA sequence/secondary structure.

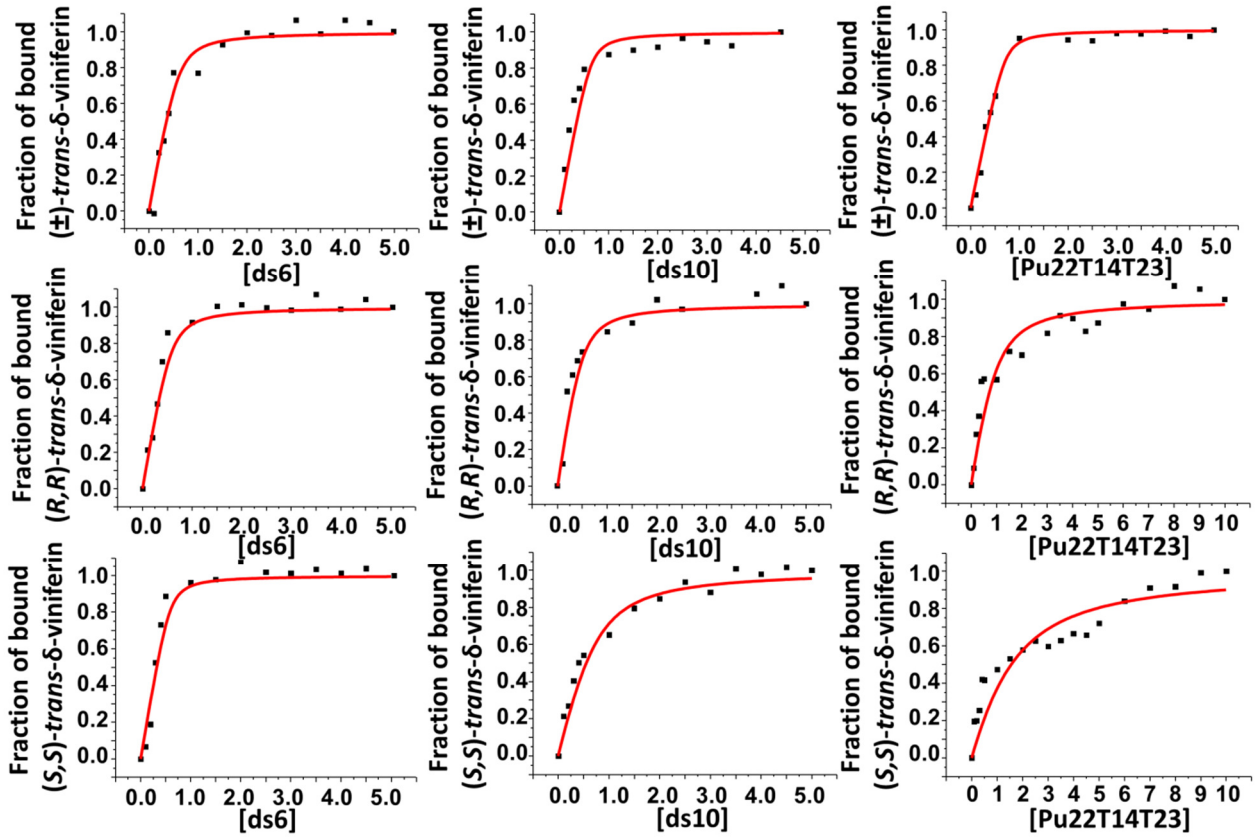


**Figure 6.** Binding curves obtained by plotting the fraction of bound (±)-*trans*-δ-viniferin, (*R,R*)-*trans*-δ-viniferin or (*S,S*)-*trans*-δ-viniferin as a function of ds6 and ds10 duplexes or Pu22T14T23 G-quadruplex concentration. The black squares represent the experimental data; the red lines are the best fits obtained with an independent and equivalent-sites model.

**Table 4.** Binding constant ($K_b$) and stoichiometry (*n*) values for complexes of each ligand with ds6 and ds10 duplexes or Pu22T14T23 G-quadruplex, obtained by fitting fluorescence data with an independent and equivalent-sites model. The errors associated to the binding constant and stoichiometry values are based on the fit.

| **Ligand/DNA target** | | **ds6** | **ds10** | **Pu22T14T23** |
|---|---|---|---|---|
| ***trans*-δ-viniferin** | **$K_b$ ($M^{-1}$)** | $(6.1\pm6.0) \times 10^6$ | $(1.1\pm1.9) \times 10^7$ | $(1.3\pm0.9) \times 10^7$ |
| | ***n*** | 3.3±0.6 | 3.1±0.7 | 2.8±0.2 |
| (*R,R*)-***trans*-δ-viniferin** | **$K_b$ ($M^{-1}$)** | $(5.7\pm5.3) \times 10^6$ | $(4.4\pm6.3) \times 10^6$ | $(1.7\pm1.5) \times 10^6$ |
| | ***n*** | 3.5±0.6 | 3.3±1.4 | 2.2±0.9 |
| (*S,S*)-***trans*-δ-viniferin** | **$K_b$ ($M^{-1}$)** | $(1.0\pm1.4) \times 10^7$ | $(1.7\pm1.0) \times 10^6$ | $(0.5\pm0.7) \times 10^6$ |
| | ***n*** | 3.4±0.6 | 2.8±0.8 | 1.8±1.7 |
| ***trans*-resveratrol** | **$K_b$ ($M^{-1}$)** | $(1.6\pm1.4) \times 10^6$ | $(1.6\pm1.3) \times 10^6$ | $(1.2\pm0.6) \times 10^6$ |

| | | | | |
|---|---|---|---|---|
| | ***n*** | 1.2±0.5 | 1.3±0.5 | 0.9±0.3 |
| ***trans*-pterostilbene** | **$K_b$ ($M^{-1}$)** | $(1.2\pm0.5)\times10^6$ | $(1.6\pm0.9)\times10^6$ | $(3.9\pm0.9)\times10^6$ |
| | ***n*** | 0.9±0.2 | 1.2±0.3 | 0.8±0.1 |
| **(±)-pterostilbene-*trans*-dihydrodimer** | **$K_b$ ($M^{-1}$)** | $(1.8\pm1.8)\times10^6$ | $(0.9\pm1.3)\times10^6$ | $(1.9\pm1.5)\times10^6$ |
| | ***n*** | 2.1±0.9 | 2.0±0.8 | 2.2±0.8 |

**Docking studies**

To get a deeper insight into the binding mode of *trans*-δ-viniferin to duplex and G-quadruplex structures, molecular docking studies were performed for (*R*,*R*)-*trans*-δ-viniferin and (*S*,*S*)-*trans*-δ-viniferin using as targets both ds10 duplex and Pu22T14T23 G-quadruplex. *trans*-Resveratrol was also studied in the complexes with the same DNA targets in order to compare the binding behaviour of *trans*-δ-viniferin with its parent compound. On the basis of the results of the fluorescence spectroscopy experiments, 1:2 or 1:1 DNA/ligand models were built for DNA/*trans*-δ-viniferin or DNA/*trans*-resveratrol complexes, respectively. In detail, the lowest energy docked conformations of the first or both the first and second most populated clusters were selected for 1:1 or 1:2 DNA/ligand systems, respectively.

As far as the interaction of (*R*,*R*)-*trans*-δ-viniferin with ds10 duplex is concerned, the most populated cluster showed poses involving the binding of the ligand in the middle region of the minor groove, while in the second most populated cluster the ligand was located in the middle region of the major groove of the duplex model. Binding energies of -7.9 and -7.7 kcal/mol were calculated for the first and second binding poses, respectively. Moreover, one hydrogen bond between O2T6 and 11,13b-OH was detected for (*R*,*R*)-*trans*-δ-viniferin bound to the middle region of the minor groove, while one hydrogen bond was found between O6G3 and 11,13a-OH for (*R,R*)-*trans*-δ-viniferin bound to the middle region of the major groove (Figures 7A and S27A,B). Conversely, the most populated cluster found for (*S*,*S*)-*trans*-δ-viniferin involved the binding of the ligand in the middle region of the major groove of ds10 duplex, while in the second most populated cluster the ligand was bound in the middle region of the minor groove of the duplex model. Binding energies of -8.0 and -8.1 kcal/mol were obtained for the first and second binding poses, respectively. Additionally, one hydrogen bond between O5'G3 and 11,13a-OH was found for (*S*,*S*)-*trans*-δ-viniferin bound to the middle region of the major groove, while three hydrogen bonds were found between O2T7 and 11,13b-OH, between O3'T6 and 11,13b-OH and between O3'A5 and 11,13b-OH for (*S*,*S*)-*trans*-δ-viniferin bound to the middle region of the minor groove (Figures 7B and S27C,D).

As far as the interaction of the pure *trans*-δ-viniferin enantiomers with Pu22T14T23 G-quadruplex is concerned, in both cases the most populated cluster involved the binding of the ligand to the 3'-end quartet, while in the second cluster the ligand was bound at the 5'-end quartet. Binding energies of -8.6 and -7.7 kcal/mol were calculated for the first and second binding poses of (*R*,*R*)-*trans*-δ-viniferin onto Pu22T14T23 G-quadruplex, respectively, while binding energies of -8.7 and -7.8 kcal/mol were found for the first and second binding poses of (*S*,*S*)-*trans*-δ-viniferin onto Pu22T14T23 G-quadruplex, respectively. π-π Stacking interactions of G13 and G18 with A2 ring of the ligand were detected for (*R*,*R*)-*trans*-δ-viniferin bound to the 3'-end quartet, while π-π stacking of G16 with A2 ring of the ligand and two hydrogen bonds between phosphate oxygen of G20 and 11,13b-OH and between O6G7 and 11,13a-OH were found for (*R,R*)-*trans*-δ-viniferin bound to the 5'-end quartet (Figures 8A and S28A,B). In turn, π-π stacking of G13 with A2 ring of the ligand and two hydrogen bonds between phosphate oxygen of T10 and 11,13b-OH and between O4T23 and 4a-OH were found for (*S*,*S*)-*trans*-δ-viniferin bound to the 3'-end quartet, while π-π stacking of G16 with B2 ring of the ligand and one hydrogen bond between the exocyclic amino group of A6 and 11,13a-OH were found for (*S*,*S*)-*trans*-δ-viniferin bound to 5'-end quartet (Figures 8B and S28C,D).

While in the ds10 duplex/*trans*-δ-viniferin systems no significant variations were detected in terms of binding energies between the two best poses at minor and major grooves, in the case of Pu22T14T23 G-quadruplex/*trans*-δ-viniferin systems a more relevant difference between binding energies for the interaction at the 3'- and 5'-end quartets was found, suggesting that the 3'-end quartet could be the preferential binding site on Pu22T14T23 G-quadruplex for both (*R,R*)-*trans*-δ-viniferin and (*S*,*S*)-*trans*-δ-viniferin.

Overall, docking results were fully consistent with binding modes inferred by NMR data for both ds10 duplex/*trans*-δ-viniferin and Pu22T14T23 G-quadruplex/*trans*-δ-viniferin complexes. Binding energies averaged over the two binding events for each DNA/*trans*-δ-viniferin system were also consistent with fluorescence-derived binding constants, showing no relevant preference of both (*R*,*R*) and (*S*,*S*) enantiomers of *trans*-δ-viniferin for the duplex or G-quadruplex targets, as well as no enantioselective binding.

Combining together the findings from NMR-derived NOE contacts, binding stoichiometries and constants derived from fluorescence spectroscopy and best docking poses and energies, four different models appear plausible for the ds10 duplex/*trans*-δ-viniferin and Pu22T14T23 G-quadruplex/*trans*-δ-viniferin complexes (Figures 7A-D and 8A-D, respectively).

As far as the *trans*-resveratrol/ds10 duplex system is concerned, the best binding pose of the ligand was in the middle region of the duplex minor groove, featured by a binding energy of -7.0 kcal/mol and forming one hydrogen bond with the duplex involving O3'T6 and 3,5-OH (Figure S29A,B). On

the other hand, the best binding pose onto Pu22T14T23 G-quadruplex was at the 3'-end quartet. A binding energy of -6.1 kcal/mol was calculated for the Pu22T14T23 G-quadruplex/*trans*-resveratrol complex, stabilized by π-π stacking of G9 and G13 with the 1,3-benzenediol ring of the ligand along with one hydrogen bond between O4T23 and 3,5-OH (Figure S29C,D). Notably, similar binding modes were observed comparing *trans*-δ-viniferin and its parent monomer *trans*-resveratrol. In full agreement with fluorescence-derived binding constants, lower binding energies were found with both targets for *trans*-resveratrol compared to *trans*-δ-viniferin.

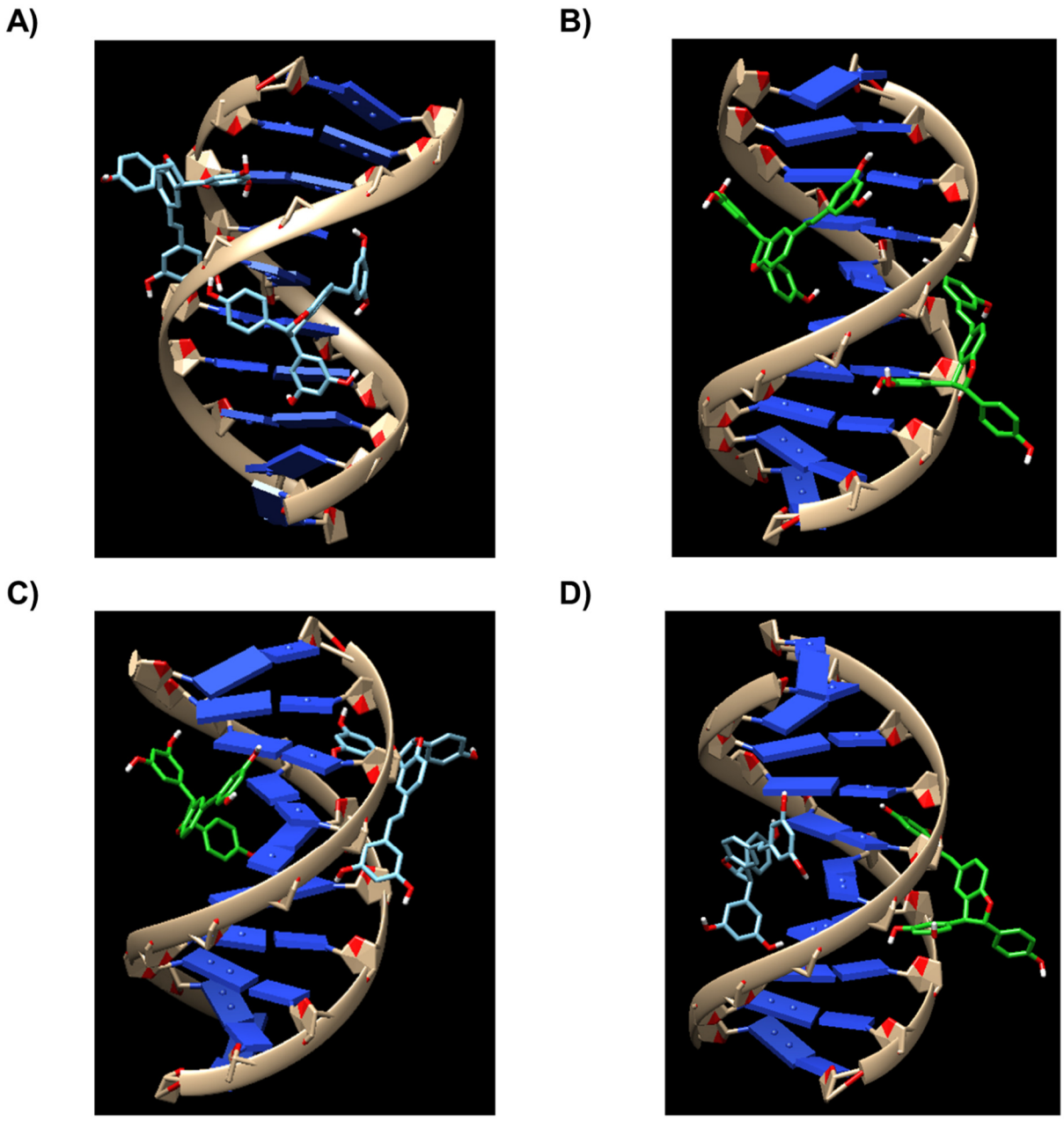


**Figure 7.** Binding mode of (*R*,*R*)-*trans*-δ-viniferin and (*S*,*S*)-*trans*-δ-viniferin when docked into ds10 duplex. The four panels represent the four possible 1:2 DNA/ligand complexes which can be formed between ds10 duplex and the two enantiomers targeting the minor and/or major grooves as follows: A) minor groove: (*R*,*R*)-*trans*-δ-viniferin, major groove: (*R*,*R*)-*trans*-δ-viniferin, B) minor groove: (*S*,*S*)-*trans*-δ-viniferin, major

groove: (*S*,*S*)-*trans*-δ-viniferin, C) minor groove: (*R*,*R*)-*trans*-δ-viniferin, major groove: (*S*,*S*)-*trans*-δ-viniferin and D) minor groove: (*S*,*S*)-*trans*-δ-viniferin, major groove: (*R*,*R*)-*trans*-δ-viniferin. (*R*,*R*)-*trans*-δ-viniferin and (*S*,*S*)-*trans*-δ-viniferin are represented as cyan and green sticks, respectively.

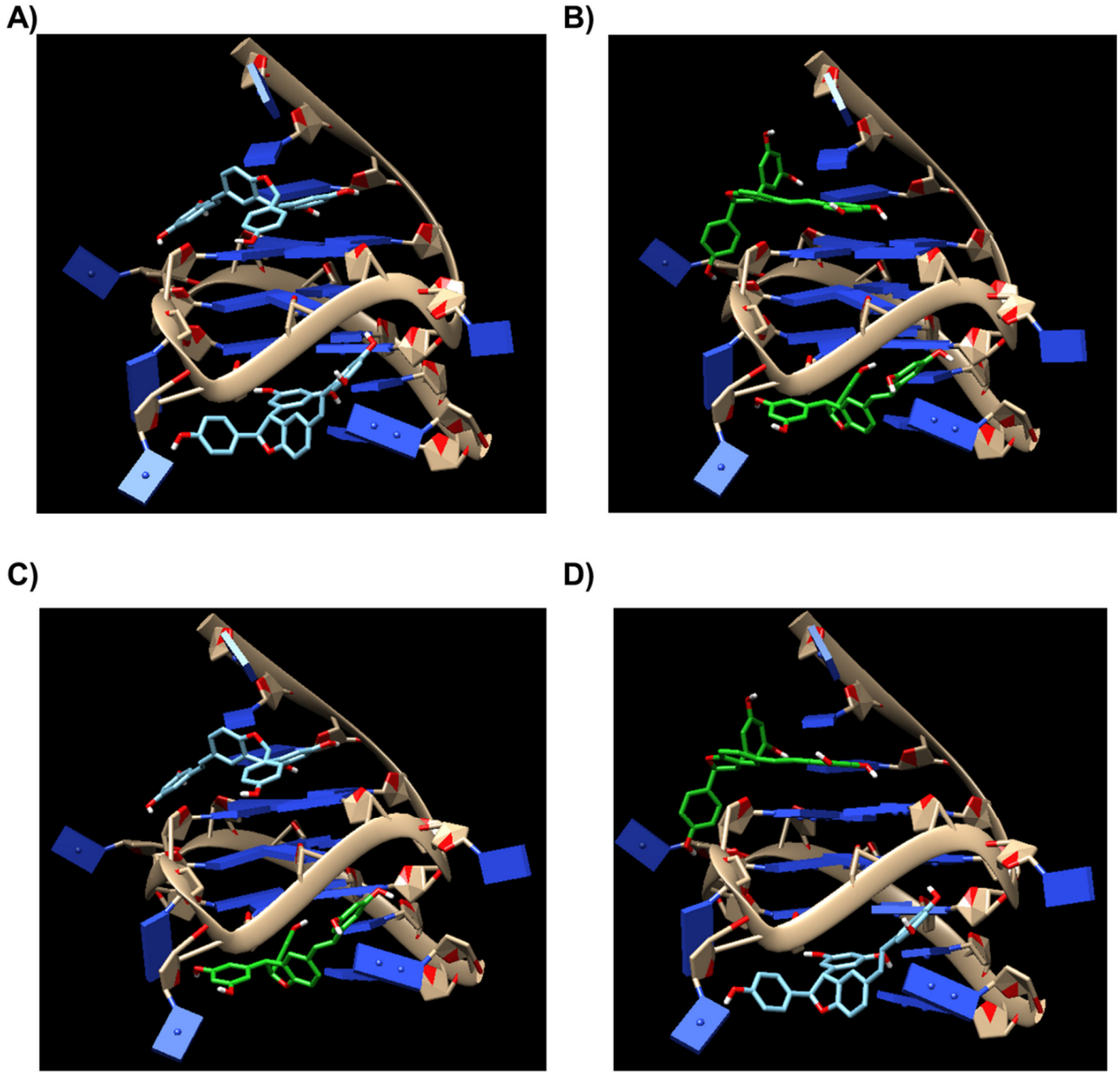


**Figure 8.** Binding mode of (*R*,*R*)-*trans*-δ-viniferin and (*S*,*S*)-*trans*-δ-viniferin when docked into Pu22T14T23 G-quadruplex. The four panels represent the four possible 1:2 DNA/ligand complexes which can be formed between Pu22T14T23 G-quadruplex and the two enantiomers targeting the 5'-end quartet (top) and/or the 3'-end quartet (bottom) as follows: A) 5'-end quartet: (*R*,*R*)-*trans*-δ-viniferin, 3'-end quartet: (*R*,*R*)-*trans*-δ-viniferin, B) 5'-end quartet: (*S*,*S*)-*trans*-δ-viniferin, 3'-end quartet: (*S*,*S*)-*trans*-δ-viniferin, C) 5'-end quartet: (*R*,*R*)-*trans*-δ-viniferin, 3'-end quartet: (*S*,*S*)-*trans*-δ-viniferin and D) 5'-end quartet: (*S*,*S*)-*trans*-δ-viniferin, 3'-end quartet: (*R*,*R*)-*trans*-δ-viniferin. (*R*,*R*)-*trans*-δ-viniferin and (*S*,*S*)-*trans*-δ-viniferin are represented as cyan and green sticks, respectively.

**Antiproliferative activity evaluation**

(±)-*trans*-δ-Viniferin, *trans*-resveratrol, *trans*-pterostilbene and (±)-pterostilbene-*trans*-dihydrodimer were tested on a panel of human tumor cell lines, i.e. melanoma A375, non-small cell lung cancer H460 and prostate cancer PC3, as well as on human normal skin WS1 fibroblasts. The antiproliferative potency of the compounds was evaluated after 48 h exposure using the MTS cell proliferation assay, and the $IC_{50}$ values were determined as the concentrations of compound causing 50% cell growth inhibition.

Among the tumor cell lines considered, H460 cells were overall the most sensitive ones. Conversely, PC3 cells resulted the least sensitive cells (Table 5). The most active compound on tumor cell lines was (±)-pterostilbene-*trans*-dihydrodimer. The compound resulted 1.75- and 1.3-fold more active than *trans*-resveratrol and *trans*-pterostilbene, respectively, on A375, about 2.3-fold more active than *trans*-resveratrol and *trans*-pterostilbene on PC3 cells, and showed cytotoxic potency similar to *trans*-resveratrol and *trans*-pterostilbene on H460 cells. Comparing the cytotoxic potency produced on WS1 fibroblasts, *trans*-resveratrol showed the highest selectivity ($IC_{50}$ > 200 μM on WS1) and (±)-pterostilbene-*trans*-dihydrodimer showed about 2-fold (PC3) and 3-fold (A375 and H460) higher cytotoxicity on tumor cells. Conversely, (±)-*trans*-δ-viniferin showed a similar cytotoxic profile on all the tested cell lines ($IC_{50}$ in the range 69-120 μM).

**Table 5.** Cytotoxic activity of the here investigated natural stilbenoids[a].

| **Compound** | **A375** | **H460** | **PC3** | **WS1** |
|---|---|---|---|---|
| | | **$IC_{50}$ (μM)[b]** | | |
| (±)-*trans*-δ-viniferin | 95±7 | 81±4 | 120±7.8 | 69±5.6 |
| *trans*-resveratrol | 44.5±3.5 | 25±0.77 | >100 | >200 |
| *trans*-pterostilbene | 33±0.7 | 25±0.4 | 97±4.9 | 57±10 |
| (±)-pterostilbene-*trans*-dihydrodimer | 25.5±2.12 | 24.7±0.35 | 42.7±0.5 | 82.7±1.06 |

[a]24 h after seeding, cells were exposed for 48 h to the compounds and cytotoxicity was measured using MTS assay. Data represent mean values ±SD of three independent experiments.
[b]$IC_{50}$ is defined as the concentration of compound causing 50% cell growth inhibition.

To evaluate the ability of the selected molecules to produce DNA damage, the expression of γ-H2AX after compound exposure was evaluated in all the cell lines. Chromatin is composed by DNA wrapping around histone octamers and forming the nucleosome. Among the histones, H2AX plays a pivotal role in nucleosome formation, chromatin remodeling and DNA repair. Phosphorylation of the Ser-139 residue of the histone H2AX, leading to γ-H2AX, is an early cellular response useful in

monitoring the induction of DNA double-strand breaks. The detection and measure of γ-H2AX levels emerged as a highly specific and sensitive molecular marker for monitoring DNA breaks induced by γ-radiation and antitumor drugs.[43] Cells were exposed for 48 h to the studied compounds at a concentration corresponding to their respective $IC_{50}$ and the level of γ-H2AX was evaluated by Western blot assay (Figure 9A). The level of DNA damage was defined by densitometric analysis. Actin/β-tubulin was used to define the relative expression levels by measuring the ratio between the band intensity of γ-H2AX and the corresponding band intensity of actin/β-tubulin (Figure 9B). Low level of DNA damage was evidenced in normal WS1 fibroblasts exposed to 200 μM *trans*-resveratrol. This behavior confirms a previous work demonstrating that *trans*-resveratrol employed at similar doses on normal or cancer cells has no effects on the former ones.[30] (±)-*trans*-δ-Viniferin, *trans*-pterostilbene, as well as (±)-pterostilbene-*trans*-dihydrodimer produced DNA damage in all the considered cell lines, with (±)-pterostilbene-*trans*-dihydrodimer being the most active DNA damaging compound of the series. These results are in agreement with the above reported NMR and fluorescence spectroscopy experiments, which proved a tight interaction between the explored ligands and both duplex- and G-quadruplex-forming DNA oligonucleotides. The lack of linear correlations between $IC_{50}$ values and observed DNA damage is not surprising, considering that multiple factors, including the recently reported repair mechanisms triggered by stilbenoids themselves, can be involved in determining the overall cytotoxicity.[28]

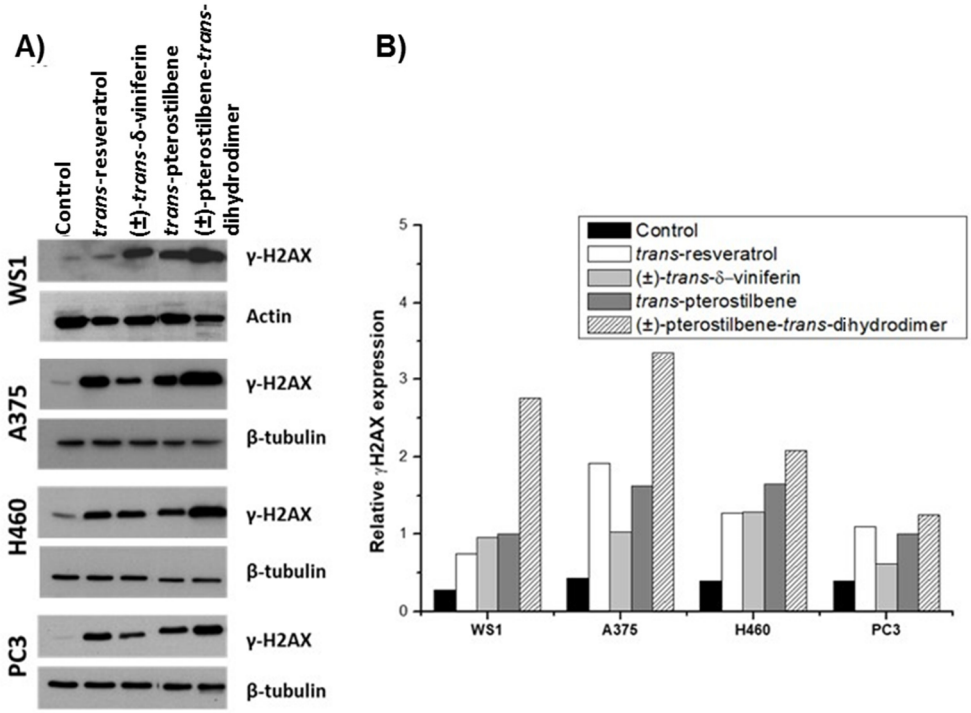


**Figure 9.** Compound-mediated DNA damage. A) The capability of the compounds to produce DNA damage was evaluated in Western blot assay by measuring the level of γ-H2AX before and after compound exposure. After seeding, cells were exposed to compounds for 48 h at concentrations corresponding to their $IC_{50}$ values. Cells were harvested for protein extraction and cell lysates were fractionated on SDS-PAGE. Actin or β-tubulin

were used as control for loading. B) The level of DNA damage was measured by densitometric analysis. The band intensity quantitation of the γ-H2AX and actin/β-tubulin were used to define the relative expression levels (ratio between the band intensity of γ-H2AX and the corresponding band intensity of actin/β-tubulin).

## Discussion

DNA is one of the main targets for anticancer drugs. Indeed, the possibility of finely modulating typical mechanisms of cancer cells acting at the genome level represents a fascinating therapeutic strategy offering several effective precedents described in the literature.[44–48] Among them, one of the most representative cases is cisplatin, a well-known and widely used chemotherapeutic agent, whose ability to bind the N7 reactive center on purine residues included in duplex DNA is associated to DNA damage, blocking of cell division and apoptotic death of cancer cells.[49,50] In the last decades, novel anticancer strategies have been conceived targeting different DNA secondary structures, particularly non-canonical structures known as G-quadruplexes.[51] G-quadruplexes are mainly found in cancer-related genomic regions, such as oncogene promoters and telomeres. Stabilizing G-quadruplexes or inducing their formation in the genome can block specific pathways of cancer cells, thus resulting in a selective action against malignant cells, which in principle can fully preserve healthy cells. Several duplex and/or G-quadruplex ligands, mostly synthetic compounds, have been thus analyzed in preclinical and clinical studies.[52–57] Conversely, few studies are reported for naturally occurring compounds.[29,30,58] In this frame, the ability of *trans*-resveratrol to interact with DNA duplex and G-quadruplex structures was recently investigated.[29,30] Notably, the ability to interact with DNA observed for this compound proved to be one of the mechanisms involved in its anticancer activity.

Based on these findings, we investigated the DNA targeting ability and the cytotoxic activity on cancer and normal cells of *trans*-resveratrol dimeric analogue (±)-*trans*-δ-viniferin. Dimeric analogues, compared to their monomeric counterpart, can represent precious scaffolds of major interest due to their more extended surface and higher number of functional moieties, which can confer higher selectivity in the recognition of biologically relevant macromolecules.

NMR analysis along with docking studies allowed building molecular models for the complexes formed between the duplex/G-quadruplex target of choice and (±)-*trans*-δ-viniferin. Intercalative and groove binding modes could be fully excluded in its interaction with the here investigated duplex (ds6 and ds10) and G-quadruplex (Pu22T14T23) models, respectively. The ligand was located in the middle regions of both minor and major grooves of the ds6 and ds10 duplexes, and the interaction was mainly stabilized by hydrogen bonds. As far as the Pu22T14T23 G-quadruplex is concerned, the binding of (±)-*trans*-δ-viniferin did not disrupt its original fold, even if rearrangements of its flanking residues covering the external quartets were observed as a consequence of the ligand binding at both

the 3'- and 5'-end quartets through stacking mode. In detail, the binding of (±)-*trans*-δ-viniferin at the 5'-end occurred through stacking interactions on the most accessible guanine of the upper quartet, i.e. G16, and no relevant rearrangement of the 5'-end flanking residues was necessary to stably accommodate the ligand onto this quartet. This was proved by the absence of significant chemical shift variations for the flanking residue A6 as well as for the upper quartet residues G7, G11 and G20. Conversely, the upfield shift for G16 was fully consistent with additional stacking interactions provided by the bound ligand, absent on the uncovered G16 of the free G-quadruplex. On the other hand, the binding of (±)-*trans*-δ-viniferin at the 3'-end occurred by stacking on G9, G13, G18 and G22 accompanied by a rearrangement of T23, A24 and A25. In particular, upon addition of the ligand, the downfield shifts experimented by G9, G13, G22, T23, A24 and A25 revealed their partial de-stacking, whereas the upfield shift of G18 indicated additional stacking interactions, absent in the free G-quadruplex. These findings indicated that the ligand was located over G9, G13, G18 and G22, thus covering the previously uncovered G18 and hampering the original direct stacking of T23 on G22 and A25 on G9. Notably, the binding of (±)-*trans*-δ-viniferin at the 3'-end of the G-quadruplex model was found to be energetically preferred over the 5'-binding, as suggested by molecular docking. This could be probably due to the favourable rearrangement of the 3'-end flanking residues which together with the lower quartet might form a peculiar pocket for the binding of the ligand. On the other hand, perturbations of $^{1}$H NMR signals belonging to the residues forming the middle quartet could be the result of a slight modification of the original stacking geometry of both the upper and lower quartets on the middle one upon ligand binding.

CD analysis confirmed that the folds of the three investigated oligonucleotide targets were not perturbed by the ligand, providing a further indication that intercalation did not occur in the duplex structures and that the parallel fold of the G-quadruplex model was preserved upon ligand binding. Moreover, CD-melting experiments proved the ability of (±)-*trans*-δ-viniferin to stabilize – even though to a limited extent – both duplex and G-quadruplex models. Fluorescence analysis demonstrated the high affinity of (±)-*trans*-δ-viniferin for both duplex and G-quadruplex structures. Additionally, fluorescence-derived binding stoichiometries, along with NMR data, suggested that two ligand molecules were involved in the binding, by targeting both the minor and major grooves of the duplex models, as well as both the 3'- and 5'-end quartets of the G-quadruplex model. In few cases, binding stoichiometries of 1:3 DNA/ligand were observed. These complexes of higher stoichiometries were probably obtained due to a third molecule of (±)-*trans*-δ-viniferin, not detected by NMR, thus probably binding to different sites on each macromolecule in a weak and unspecific manner. Investigation of pure (*R*,*R*) and (*S*,*S*) enantiomers of *trans*-δ-viniferin did not show relevant differences in targeting duplex and G-quadruplex structures with respect to the racemic mixture.

Interestingly, comparing (±)-*trans*-δ-viniferin with its parent compound *trans*-resveratrol, it emerged that the dimeric stilbenoid had higher affinity towards the DNA targets than the monomeric species. Similar binding modes were observed for both ligands in the interaction with duplex and G-quadruplex structures, though 1:1 DNA/ligand complexes were consistently formed by *trans*-resveratrol.

The methoxylated analogues of (±)-*trans*-δ-viniferin and *trans*-resveratrol, i.e. (±)-pterostilbene-*trans*-dihydrodimer and *trans*-pterostilbene, respectively, showed similar binding modes, affinities and stoichiometries with all the DNA targets compared to their parent analogues, in line with their structural similarities.

All the compounds were cytotoxic in the μM concentration range on a panel of cancer cell lines and produced DNA damage, consistent with their interaction with both DNA duplex and G-quadruplex structures. Thus, DNA damaging activity could be considered one of the mechanisms of action of these stilbenoids responsible for their cytotoxicity, even if additional mechanisms involving other targets cannot be excluded, in accordance with previous reports in the literature.[29,30]

With the aim of synthesizing more active and selective DNA-binding ligands based on natural stilbenoids, the design of novel dimeric and monomeric analogues has been now actively undertaken in our laboratories. The molecular models here built for the complexes of (±)-*trans*-δ-viniferin and *trans*-resveratrol with DNA duplex and G-quadruplex structures are indeed a precious source of inspiration taking into account the unique features of the ligands in their bound conformations for an effective optimization process.

## Experimental section

### Chemistry

Oligonucleotide sequences d(CGTACG), d(AAGAATTCTT) and d(TGAGGGTGGGTAGGGTGGGTAA) were purchased from Eurofins Genomics. The oligonucleotide concentration was determined by measuring the absorbance at 260 nm and 90 °C, using the appropriate molar extinction coefficients. (±)-*trans*-δ-Viniferin, (*R,R*)-*trans*-δ-viniferin, (*S,S*)-*trans*-δ-viniferin, *trans*-resveratrol, *trans*-pterostilbene and (±)-pterostilbene-*trans*-dihydrodimer were synthesized and purified as previously reported.[31,32] The ligand stock solutions were prepared by dissolving the solid compounds in DMSO-d6 at 26 mM concentration of the ligand for NMR studies or in DMSO at 2 mM concentration for CD and fluorescence analyses.

**NMR experiments**

The NMR samples of self-complementary oligonucleotides forming duplexes ds6 and ds10 were prepared at 0.30 mM concentration. Both sequences adopt a B-DNA double helix conformation in $H_2O/D_2O$ (9:1), 100 mM NaCl, 10 mM sodium phosphate buffer (pH 7.0), as previously determined.[59,60] The NMR sample of Pu22T14T23 was prepared at 0.34 mM concentration in a $H_2O/D_2O$ (9:1), 70 mM KCl, 25 mM potassium phosphate buffer (pH 6.9). Pu22T14T23 sample was heated to 85 °C for 1 min and then cooled at room temperature overnight.

The NMR spectra were recorded on a Bruker AV600 spectrometer operating at a frequency of 600.10 MHz and 242.94 MHz, for $^{1}H$ and $^{31}P$ nuclei, respectively. NMR titrations were performed by adding increasing amounts of ligand to the DNA samples at different ratios R = [(±)-*trans*-δ-viniferin]/[DNA] from R = 0 to R = 2.0. The $^{1}H$ and $^{31}P$ assignments for the free oligonucleotides ds6 and ds10 have been previously reported.[59,60] Proton resonance assignments of the free Pu22T14T23 sequence were performed on the basis of previous assignments.[23,37] The protons of duplex and G-quadruplex-forming oligonucleotides in the complexes were assigned using standard NOESY and TOCSY experiments. (±)-*trans*-δ-Viniferin protons were assigned by an integrated series of 2D experiments such as ROESY, TOCSY and COSY. Phase sensitive NOESY spectra of the complexes were acquired at 15 °C or 25 °C, for the duplexes and the G-quadruplex respectively, in TPPI mode, with 2048 × 1024 complex FIDs. Mixing times ranged from 150 to 300 ms. TOCSY spectra were acquired with the use of a MLEV-17 spin-lock pulse (60 ms total duration). All spectra were transformed and weighted with a 90° shifted sine-bell squared function to 4K × 4K real data points.

**CD experiments**

CD spectra were recorded on a Jasco J-715 spectropolarimeter equipped with a Peltier-type temperature control system (model PTC-348WI), using a quartz cuvette with a path length of 1 cm. The spectra were recorded at 15 °C for the ds6 and ds10 duplexes and 25 °C for Pu22T14T23 G-quadruplex, in the range 220-600 nm with 2 s response, 50 nm/min scanning speed, 2.0 nm bandwidth, and corrected by subtraction of the background scan with buffer. All the spectra were averaged over 3 scans. The ds6 and ds10 samples were dissolved in 100 mM NaCl, 10 mM sodium phosphate buffer (pH 7.0), while Pu22T14T23 was dissolved in 70 mM KCl, 25 mM potassium phosphate buffer (pH 6.9) or 5 mM KCl, 5 mM potassium phosphate buffer (pH 6.9), to obtain 2 μM solutions. The Pu22T14T23 sample was then annealed by heating at 85 °C for 1 min, followed by slow cooling to room temperature. CD titrations were obtained by adding increasing amounts of each ligand to ds6 and ds10 duplexes or Pu22T14T23 G-quadruplex. Each ligand was added to each oligonucleotide solution up to 4 molar equivalents. After each ligand addition, the system was

allowed equilibrating before recording the spectrum. For the CD-melting experiments, ellipticity was recorded at 257, 248 or 265 nm for ds6 and ds10 duplexes or Pu22T14T23 G-quadruplex, respectively, in the absence and presence of 4 molar equivalents of each ligand, with a temperature scan rate of 0.5 °C/min in the range 10-95 °C.

**Fluorescence experiments**

Fluorescence spectra were recorded on HORIBA JobinYvon Inc. FluoroMax®-4 spectrofluorimeter equipped with F-3004 Sample Heater/Cooler Peltier Thermocouple Drive, using a quartz cuvette with a 1 cm path length. For the fluorescence titration experiments with (±)-*trans*-δ-viniferin**,** (*R,R*)-*trans*-δ-viniferin and (*S,S*)-*trans*-δ-viniferin, an excitation wavelength of 309 nm was used; for the fluorescence titration experiments with *trans*-resveratrol, *trans*-pterostilbene and (±)-pterostilbene-*trans*-dihydrodimer, excitation wavelengths of 305, 306 and 341 nm were used, respectively. The spectra were recorded at 15 °C for ds6 and ds10 duplexes and 25 °C for Pu22T14T23 G-quadruplex systems, in the range 315-550 nm for (±)-*trans*-δ-viniferin, (*R,R*)-*trans*-δ-viniferin and (*S,S*)-*trans*-δ-viniferin, 310-550 nm for *trans*-resveratrol and *trans*-pterostilbene, and 345-550 nm for (±)-pterostilbene-*trans*-dihydrodimer. Titrations were carried out at a fixed concentration of each ligand, i.e. 2.0 μM. The ligands were dissolved in 100 mM NaCl, 10 mM sodium phosphate buffer (pH 7.0) for titrations with ds6 and ds10 duplexes and in 70 mM KCl, 25 mM potassium phosphate buffer (pH 6.9) for titrations with Pu22T14T23 G-quadruplex. The ds6 and ds10 duplexes were dissolved in 100 mM NaCl, 10 mM sodium phosphate buffer (pH 7.0), while Pu22T14T23 was dissolved in 70 mM KCl, 25 mM potassium phosphate buffer (pH 6.9), to obtain 120 μM solutions. The Pu22T14T23 sample was then annealed by heating at 85 °C for 1 min, followed by slow cooling to room temperature. Increasing amounts of ds6 and ds10 duplexes or Pu22T14T23 G-quadruplex were added to the 2 μM ligand solutions from the corresponding 120 μM stock solutions. Each DNA solution was added to the tested ligand solution until a plateau in fluorescence intensity was reached, which corresponded to 5 or 10 μM DNA concentration.

The fraction of bound ligand was calculated from the fluorescence intensity at 389 nm for (±)-*trans*-δ-viniferin, (*R,R*)-*trans*-δ-viniferin, (*S,S*)-*trans*-δ-viniferin and (±)-pterostilbene-*trans*-dihydrodimer, or 383 nm for *trans*-resveratrol and *trans*-pterostilbene. The data were then reported in the graph as a function of the DNA concentration. The obtained points were then fitted with an independent and equivalent-sites model,[40] using the Origin 8.0 program, with the following equation:

$$\alpha = \left(\frac{1}{2[L]_0}\right)\left\{\left([L]_0 + n[Qu] + \frac{1}{K_b}\right) - \sqrt{\left([L]_0 + n[Qu] + \frac{1}{K_b}\right)^2 - 4[L]_0 n[Qu]}\right\}$$

where α is the mole fraction of ligand in the bound form, $[L]_0$ is the total ligand concentration, $[Qu]$ is the added DNA concentration, $n$ is the number of the equivalent and independent sites on the DNA structure and $K_b$ is the binding constant. The fraction of the bound ligand was determined by using the following equation:

$$\alpha = \frac{Y - Y_0}{Y_b - Y_0}$$

where $Y$, $Y_0$ and $Y_b$ are the values of fluorescence emission intensity at the maximum, respectively, at each titrant concentration, at the initial state and the final state of the titration. The errors associated to the binding constant and stoichiometry values are based on the fit.

**Docking studies**

The bimolecular duplex d(AAGAATTCTT)$_2$ (ds10) was built using the Build Structure Tool within the UCSF Chimera software and minimized by setting steepest descent steps = 100 and conjugate gradient steps = 100, both with a step size of 0.02 Å. The G-quadruplex-forming oligonucleotide of sequence d(TGAGGGTGGGTAGGGTGGGTAA) (Pu22T14T23) was prepared using as starting point the NMR deposited structure of the complex Pu22T14T23/quindoline (PDB 2L7V)[36] from which the two bound quindolines were removed.

Molecular docking calculations were carried out using AutoDock Vina with the aid of its graphical user interface AutoDockTools.[61] The ligands, (*R,R*)-*trans*-δ-viniferin, (*S,S*)-*trans*-δ-viniferin and *trans*-resveratrol, and the DNA targets were prepared by use of AutoDockTools and UCSF Chimera by assigning bond orders, adding hydrogen atoms and generating the appropriate protonation states. The ligands and targets were then converted to proper Autodock PDBQT file formats and the Gaisteiger charges were assigned. The 3D grid box dimensions were defined including the whole DNA macromolecules. The docking area was centered on the DNA center of mass and grid boxes of 70 Å × 86 Å × 60 Å and 100 Å × 90 Å × 60 Å for ds10 and Pu22T14T23, respectively, with a 0.375 Å spacing, were used. 100 docking poses were generated by using as docking parameters seed = random, exhaustiveness = 24 and number of binding modes = 20 for each of the 5 runs performed for each DNA/ligand system. Docking poses were clustered on the basis of their root-mean square deviation and were ranked on the basis of binding energy. 1:2 DNA/*trans*-δ-viniferin systems were obtained by joining the best docking poses of (*R,R*)-*trans*-δ-viniferin or (*S,S*)-*trans*-δ-viniferin at the two different binding sites on each target. Molecular modeling figures were drawn by UCSF Chimera.

**Cell lines**

The human skin normal fibroblast WS1 (ATCC CRL-1502) cells were cultured in Eagle's Minimum Essential Medium plus 10% FBS at 37 °C and 5% $CO_2$. The human malignant melanoma A375

(ATCC CRL-1619) cells were cultured in Dulbecco's Modified Eagle's Medium plus 10% FBS at 37 °C and 5% $CO_2$. The non-small cell lung cancer NCI-H460 (ATCC HTB-177) and prostate cancer PC-3 (ATCC CRL-1435) cells were cultured in RPMI 1460 plus 10% FBS at 37 °C and 5% $CO_2$.

**Cytotoxicity assay**

Cytotoxic potency of the compounds was assessed by growth inhibition assay (CellTiter 96® AQueous One Solution Cell Proliferation Assay MTS, Promega). Cells were seeded in 96-well plates and after 24 h exposed to the compounds (concentration range 1-100/200 μM). After 48 h exposure, 20 μL of a MTS (3-(4,5-dimethylthiazol-2-yl)-5-(3-carboxymethoxyphenyl)-2-(4-sulfophenyl)-2H-tetrazolium salt) solution were added to each well. The absorbance was measured using a FLUOstar OPTIMA plate reader (BMG Labtech GmbH, Offenburg, Germany) at 492 nm after 4 h incubation at 37 °C in 5% $CO_2$. $IC_{50}$ values were determined as the drug concentration causing 50% cell growth inhibition, obtained by dose-response curves. Experiments were performed in triplicate.

**Western blot assay**

24 h after seeding, cells were exposed to compounds for 48 h at concentrations corresponding to their respective $IC_{50}$ values. Cells were harvested and lysated. Samples were loaded on SDS-PAGE and then transferred on nitrocellulose film. Membranes were blocked with 5% w/v nonfat dry milk and incubated with primary antibody followed with HRP-conjugated secondary antibody and detected by chemiluminescence (ECL, Amersham). The levels of actin and β-tubulin were used as control for loading.

**Acknowledgements**

C.P. was supported by a FIRC-AIRC fellowship for Italy.

**REFERENCES**

[1] C. M. Galanakis, *Polyphenols: Properties, Recovery, and Applications*, Woodhead Publishing, **2018**.
[2] S. Quideau, D. Deffieux, C. Douat-Casassus, L. Pouységu, *Angew. Chemie - Int. Ed.* **2011**, *50*, 586–621.
[3] R. Tsao, *Nutrients* **2010**, *2*, 1231–1246.
[4] D. B. Niesen, C. Hessler, N. P. Seeram, *J. Berry Res.* **2013**, *3*, 181–196.
[5] P. Jeandet, B. Delaunois, A. Conreux, D. Donnez, V. Nuzzo, S. Cordelier, C. Clément, E. Courot, *BioFactors* **2010**, *36*, 331–341.
[6] B. C. Akinwumi, K. A. M. Bordun, H. D. Anderson, *Int. J. Mol. Sci.* **2018**, *19*, 1–25.
[7] S. Weiskirchen, R. Weiskirchen, *Adv. Nutr. An Int. Rev. J.* **2016**, *7*, 706–718.
[8] J. Gambini, M. Inglés, G. Olaso, R. Lopez-Grueso, V. Bonet-Costa, L. Gimeno-Mallench, C. Mas-Bargues, K. M. Abdelaziz, M. C. Gomez-Cabrera, J. Vina, C. Borras, *Oxid. Med. Cell. Longev.* **2015**, *2015*, ID 837042.

[9] W.-S. Lin, J. V. Leland, C.-T. Ho, M.-H. Pan, *J. Agric. Food Chem.* **2020**, *68*, 12788–12799.
[10] Y. Liu, Y. You, J. Lu, X. Chen, Z. Yang, *Molecules* **2020**, *25*, 5166.
[11] P. Penãlver, S. Zodio, R. Lucas, M. V. De-Paz, J. C. Morales, *J. Agric. Food Chem.* **2020**, *68*, 1609–1620.
[12] A. Kumar, A. S. Levenson, in *Epigenetics Cancer Prev.*, **2019**, pp. 169–186.
[13] C. K. Singh, M. A. Ndiaye, N. Ahmad, *Biochim. Biophys. Acta* **2015**, *1852*, 1178–1185.
[14] A. R. Guthrie, H. H. S. Chow, J. A. Martinez, *Pharmacol. Res. Perspect.* **2017**, *5*, e00294.
[15] Y. H. Lee, Y. Y. Chen, Y. L. Yeh, Y. J. Wang, R. J. Chen, *Int. J. Mol. Sci.* **2019**, *20*, 2716.
[16] J. K. Aluyen, Q. N. Ton, T. Tran, A. E. Yang, H. B. Gottlieb, R. A. Bellanger, *J. Diet. Suppl.* **2012**, *9*, 45–56.
[17] D. McCormack, D. McFadden, *J. Surg. Res.* **2012**, *173*, e53–e61.
[18] S. Fulda, *Drug Discov. Today* **2010**, *15*, 757–765.
[19] D. Rhodes, H. J. Lipps, *Nucleic Acids Res.* **2015**, *43*, 8627–8637.
[20] S. Asamitsu, S. Obata, Z. Yu, T. Bando, H. Sugiyama, *Molecules* **2019**, *24*, 429.
[21] S. Burge, G. N. Parkinson, P. Hazel, A. K. Todd, S. Neidle, *Nucleic Acids Res.* **2006**, *34*, 5402–5415.
[22] A. Siddiqui-Jain, C. L. Grand, D. J. Bearss, L. H. Hurley, *Proc. Natl. Acad. Sci. U. S. A.* **2002**, *99*, 11593–11598.
[23] L. Musso, S. Mazzini, A. Rossini, L. Castagnoli, L. Scaglioni, R. Artali, M. Di Nicola, F. Zunino, S. Dallavalle, *Biochim. Biophys. Acta - Gen. Subj.* **2018**, *1862*, 615–629.
[24] P. Agrawal, C. Lin, R. I. Mathad, M. Carver, D. Yang, *J. Am. Chem. Soc.* **2014**, *136*, 1750–1753.
[25] H. J. Lipps, D. Rhodes, *Trends Cell Biol.* **2009**, *19*, 414–422.
[26] F. A. Lagunas-Rangel, R. M. Bermúdez-Cruz, *Front. Oncol.* **2020**, *10*, 1–13.
[27] D. J. Colin, E. Limagne, K. Ragot, G. Lizard, F. Ghiringhelli, Solary, B. Chauffert, N. Latruffe, D. Delmas, *Cell Death Dis.* **2014**, *5*, e1533.
[28] T. Hsieh, Y. Huang, J. M. Wu, *Carcinogenesis* **2011**, *32*, 93–101.
[29] C. Platella, S. Guida, L. Bonmassar, A. Aquino, E. Bonmassar, G. Ravagnan, D. Montesarchio, G. N. Roviello, D. Musumeci, M. P. Fuggetta, *Biochim. Biophys. Acta - Gen. Subj.* **2017**, *1861*, 2843–2851.
[30] C. Platella, U. Raucci, N. Rega, S. D'Atri, L. Levati, G. N. Roviello, M. P. Fuggetta, D. Musumeci, D. Montesarchio, *Int. J. Biol. Macromol.* **2020**, *151*, 1163–1172.
[31] L. M. Mattio, S. Dallavalle, L. Musso, R. Filardi, L. Franzetti, L. Pellegrino, P. D'Incecco, D. Mora, A. Pinto, S. Arioli, *Sci. Rep.* **2019**, *9*, 19525.
[32] L. M. Mattio, M. Marengo, C. Parravicini, I. Eberini, S. Dallavalle, *Molecules* **2019**, *24*, 3225.
[33] A. Wilkens, J. Paulsen, V. Wray, P. Winterhalter, *J. Agric. Food Chem.* **2010**, *58*, 6754–6761.
[34] D. G. Gorenstein, *Phosphorus-31 NMR. Principles and Applications*, New York, **1984**.
[35] M. Misiak, M. Heldt, M. Szeligowska, S. Mazzini, L. Scaglioni, G. J. Grabe, M. Serocki, J. Lica, M. Switalska, J. Wietrzyk, G. L. Beretta, P. Perego, D. Zietkowski, M. Baginski, E. Borowski, A. Skladanowski, *Oncotarget* **2017**, *8*, 105137–105154.
[36] J. Dai, M. Carver, L. H. Hurley, D. Yang, *J. Am. Chem. Soc.* **2011**, *133*, 17673–17680.
[37] A. Ambrus, D. Chen, J. Dai, R. A. Jones, D. Yang, *Biochemistry* **2005**, *44*, 2048–2058.
[38] R. del Villar-Guerra, J. O. Trent, J. B. Chaires, *Angew. Chemie - Int. Ed.* **2018**, *57*, 7171–7175.
[39] J. Kypr, I. Kejnovská, D. Renčiuk, M. Vorlíčková, *Nucleic Acids Res.* **2009**, *37*, 1713–1725.
[40] C. Giancola, B. Pagano, *Top. Curr. Chem.* **2013**, *330*, 2011–242.
[41] C. Platella, M. Trajkovski, F. Doria, M. Freccero, J. Plavec, D. Montesarchio, *Nucleic Acids Res.* **2020**, *48*, 12380–12393.
[42] I. Buchholz, B. Karg, J. Dickerhoff, A. Sievers-Engler, M. Lämmerhofer, K. Weisz, *Chem. - A Eur. J.* **2017**, *23*, 5814–5823.
[43] L. J. Mah, A. El-Osta, T. C. Karagiannis, *Leukemia* **2010**, *24*, 679–686.
[44] N. S. Gavande, P. S. Vandervere-Carozza, H. D. Hinshaw, S. I. Jalal, C. R. Sears, K. S.

Pawelczak, J. J. Turchi, P. T. Author, *Pharmacol. Ther.* **2016**, *160*, 65–83.
[45] L. H. Hurley, *Nat. Rev. Cancer* **2002**, *2*, 188–200.
[46] J. Sun, Q. Wei, Y. Zhou, J. Wang, Q. Liu, H. Xu, *BMC Syst. Biol.* **2017**, *11*, 87.
[47] S. Crisci, F. Amitrano, M. Saggese, T. Muto, S. Sarno, S. Mele, P. Vitale, G. Ronga, M. Berretta, R. Di Francia, *Medicina (B. Aires).* **2019**, *55*, 414.
[48] G. Cimino-Reale, N. Zaffaroni, M. Folini, *Curr. Pharm. Des.* **2016**, *22*, 6612–6624.
[49] S. Dasari, P. Bernard Tchounwou, *Eur. J. Pharmacol.* **2014**, 364–378.
[50] S. Rottenberg, C. Disler, P. Perego, *Nat. Rev. Cancer* **2021**, *21*, 37–50.
[51] D. Varshney, J. Spiegel, K. Zyner, D. Tannahill, S. Balasubramanian, *Nat. Rev. Mol. Cell Biol.* **2020**, *21*, 459–474.
[52] D. Monchaud, M. P. Teulade-Fichou, *Org. Biomol. Chem.* **2008**, *6*, 627–636.
[53] C. Platella, V. Pirota, D. Musumeci, F. Rizzi, S. Iachettini, P. Zizza, A. Biroccio, M. Freccero, D. Montesarchio, F. Doria, *Int. J. Mol. Sci.* **2020**, *21*, 1964.
[54] J. Amato, C. Platella, S. Iachettini, P. Zizza, D. Musumeci, S. Cosconati, A. Pagano, E. Novellino, A. Biroccio, A. Randazzo, B. Pagano, D. Montesarchio, *Eur. J. Med. Chem.* **2019**, *163*, 295–306.
[55] D. Musumeci, J. Amato, P. Zizza, C. Platella, S. Cosconati, C. Cingolani, A. Biroccio, E. Novellino, A. Randazzo, C. Giancola, B. Pagano, D. Montesarchio, *Biochim. Biophys. Acta - Gen. Subj.* **2017**, *1861*, 1341–1352.
[56] V. Pirota, C. Platella, D. Musumeci, A. Benassi, J. Amato, B. Pagano, G. Colombo, M. Freccero, F. Doria, D. Montesarchio, *Int. J. Biol. Macromol.* **2021**, *166*, 1320–1334.
[57] M. P. O'Hagan, P. Peñalver, R. S. L. Gibson, J. C. Morales, M. C. Galan, *Chem. - A Eur. J.* **2020**, *26*, 6224–6233.
[58] J. Carvalho, J. L. Mergny, G. F. Salgado, J. A. Queiroz, C. Cruz, *Trends Mol. Med.* **2020**, *26*, 848–861.
[59] S. Mazzini, R. Mondelli, E. Ragg, *J. Chem. Soc. Perkin Transtactions 2* **1998**, 1983–1991.
[60] S. Mazzini, M. C. Bellucci, R. Mondelli, *Bioorganic Med. Chem.* **2003**, *11*, 505–514.
[61] O. Trott, A. J. Olson, *J. Comput. Chem.* **2009**, *31*, 455–461.

## Table of Contents

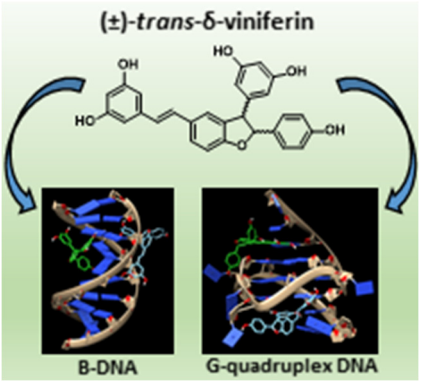


The stilbenoid (±)-*trans*-δ-viniferin**,** deriving from *trans*-resveratrol dimerization, binds to minor and major grooves of B-DNA, and to 3'- and 5'-ends of G-quadruplex DNA by stacking on the outer quartets accompanied by rearrangement of flanking residues. Consistently with ability to tightly interact with different DNA secondary structures, (±)-*trans*-δ-viniferin shows DNA damaging activity.

**Keywords**: DNA, G-quadruplexes, stilbenoids, viniferin, resveratrol.